tan, both *in vitro* and *in vivo* (*3*, *4*). The allelic frequencies for these deleterious variations differ considerably among different ethnic populations. In Caucasian populations, the frequencies of *CYP2C9*2* and *CYP2C9*3* were 8–14% and 4–16%, respectively (*5*). In contrast, *CYP2C9*2* was not present in Asian populations, and *CYP2C9*3* was present in only 1–4% of Asian populations. Therefore, interethnic variability reported in the pharmacokinetics and pharmacodynamics of drugs, metabolized mainly by CYP2C9, could not be fully explained by the common variants alone. Recently, a number of novel nonsynonymous variations of CYP2C9 have been identified in different Asian populations (*6–11*). Functional analysis of these variations *in vitro* indicated the existence in Asians of new deleterious alleles of CYP2C9 that might have clinical relevance.

Losartan, the first selective angiotensin II receptor antagonist, was reported to significantly reduce the risk of cardiovascular endpoint outcomes compared with atenolol in high-risk hypertensive patients with left ventricular hypertrophy (*12*). Large interindividual variations in the efficacy and toxicity of losartan have been reported, and it has been suggested that they are genetically determined. A relationship was suggested between the polymorphism in the receptor gene, *AGT1R*, and its humoral and renal hemodynamic responses (*13*). However, losartan is oxidized primarily by CYP2C9 to an active carboxylic acid metabolite, E-3174, which has higher potency and a longer half-life than losartan and is therefore responsible for most of the antihypertensive effects (*14*, *15*). The effects of *CYP2C9*2* and *CYP2C9*3* on losartan oxidation have been extensively studied both *in vitro* and *in vivo*, consistently demonstrating the functional defect of the *CYP2C9*3* allele in decreasing the oxidation of losartan (*16–20*). However, the clinical relevance of genotypes of *CYP2C9* to the variable blood pressure–lowering responses to losartan in hypertensive patients has not been fully clarified. Furthermore, it remains unknown whether the other deleterious CYP2C9 alleles in Asians (*6–11*) might lead to the phenotypes of impaired therapeutic responses to this drug.

We studied several genes responsible for essential hypertension and interindividual differences in responses to warfarin and antihypertensive drugs (*21*, *22*). To identify the functional mutations, we resequenced some candidate genes including *WNK4*, *SCNN1B*, *SCNN1G*, *NR3C2*, and *RGS2* for hypertension (*23–26*) and *VKORC1*, *GGCX*, and *CALU* for warfarin (*22*, *27*). In the course of this resequencing, we noticed that the deleterious mutations are present more frequently than we expected, and the rare mutations with deleterious function would increase the total phenotype change.

In the present study, we resequenced the *CYP2C9* in 724 Japanese individuals. Two novel missense mutations were functionally analyzed in the baculovirus/insect cell expression system with diclofenac as a substrate. Furthermore, we assessed the blood pressure–lowering responses to losartan in hypertensive patients with the deleterious mutations in *CYP2C9*.

Methods

Subjects

Seven hundred twenty-four Japanese subjects in this study were enrolled for genetic sequencing of *CYP2C9*. The study subjects consisted of 312 patients with stroke and 412 patients with hypertension. Stroke patients (87 females and 225 males; average age: 65.36±11.87 years; body mass index: 23.28±3.01 kg/m^2) were admitted to the Cerebrovascular Division of the National Cardiovascular Center (*22*, *28*). They had all experienced an ischemic stroke within 7 d prior to admission. Hypertensive patients (196 females and 216 males; average age: 64.83±10.42 years; body mass index: 24.55±3.69 kg/m^2) were recruited from the outpatients clinic in the Division of Hypertension and Nephrology at the National Cardiovascular Center (*23–26*, *29*). Hypertension was defined as systolic blood pressure > 140 mmHg, diastolic blood pressure >90 mmHg, or the current use of antihypertensive medication. Ninety-three percent of the study subjects (382 subjects) were diagnosed with essential hypertension, and the rest had secondary hypertension, including renal hypertension (10 subjects), renovascular hypertension (9 subjects), primary aldosteronism (7 subjects), and others (4 subjects).

Sixty-nine essential hypertensive patients (30 females and 39 males; average age: 64.36±9.34 years; body mass index: 22.65±7.84 kg/m^2) were taking one of three angiotensin II receptor blockers (losartan, candesartan, and valsartan) for treatment of hypertension. Among them, 39 patients had been receiving 50 mg/d of losartan for more than 3 months. We evaluated the patients' average resting blood pressure measured on three consecutive outpatient clinic visits, before and after losartan treatment.

The study was approved by the Ethics Review Committee of the National Cardiovascular Center, and only those subjects who provided written informed consent for genetic analyses were included in the study.

Resequencing of *CYP2C9* in 724 Japanese Subjects

Whole blood was collected from each participant, and genomic DNA was extracted from peripheral blood leukocyte. From each subject, 687 base pairs of the promoter region, all exons and intron-exon junctions, and the 3′-UTR of *CYP2C9* were amplified and sequenced directly on both strands using an ABI 3730 Automated Sequence Analyzer (Applied Biosystems, Foster City, USA), as described previously (*27*, *30*). Primers were designed to be specific to *CYP2C9*, with particular attention being paid to avoid amplification of sequences from homologous genes (*cf.* Online Table 1). The obtained sequences were examined for the presence of variations using Namihei software (Mitsui Knowl-

edge Industry Co., Ltd., Japan) and Sequencher software (Gene Codes Corporation, Ann Arbor, USA), followed by visual inspection. Novel nonsynonymous single nucleotide polymorphisms (SNPs) were confirmed by sequencing of PCR products generated from new genomic DNA amplifications. The genomic and cDNA sequences of *CYP2C9*, obtained from GenBank (NC_000010.8 and NM 000771.2, respectively), were used as reference sequences. The A of ATG of the initiator Met codon was denoted as nucleotide +1, and the initial Met residue was denoted as amino acid +1. The identified missense mutations were mapped in the human CYP2C9 crystal structure bound with warfarin (*31*) by the PyMOL v0.99 molecular visualization system (DeLano Scientific LLC, San Carlos, USA).

Cloning, Site-Directed Mutagenesis and Vector Constructions

A full-length human NADPH-cytochrome P450 oxidoreductase (OR) cDNA was isolated by PCR from human adult normal liver Quick-Clone cDNA (Clontech, Palo Alto, USA) with the forward primer, 5′-CACCAGTTTCATGATCAA CATGGG-3′, and the reverse primer, 5′-GCCCCTAGCTCC ACACGTCC-3′. The underlined sequence was introduced to the directional TOPO cloning system. The PCR products were cloned directly into the pcDNA3.1D/TOPO vector (Invitrogen, Carlsbad, USA) according to the manufacturer's instructions (pcDNA3.1D/OR). Two single *CYP2C9* variations, 3573 G>A (Arg132Gln) and 42543 G>A (Arg335Gln), were introduced into the wild-type plasmid (pcDNA3.1D/ CYP2C9/Wild-type) as a template using a QuickChange Site-Directed Mutagenesis Kit (Stratagene, La Jolla, USA). The primer sequences used for the construction of variant plasmids were as follows: 5′-CTCCCTCATGACGCTGC**A** GAATTTTGGGATGG-3′ (sense) and 5′-CCATCCCAA AATTC**T**GCAGCGTCATGAGGGAG-3′ (antisense) for pcDNA3.1D/CYP2C9/ Arg132Gln. 5′-TGATTGGCAGAA ACC**A**GAGCCCCTGCATGCA-3′ (sense) and 5′-TGCATG CAGGGGCTC**T**GGTTTCTGCCAATCA-3′ (antisense) for pcDNA3.1D/CYP2C9/ Arg335Gln.

The position of the exchanged nucleotide is underlined and in boldface. To ensure that no errors had been introduced during amplification, the entire cDNA regions were confirmed by sequencing the plasmid construct. Both OR and CYP2C9 wild-type or variant cDNAs were subcloned into the baculovirus transfer vector, pFastBac Dual (Invitrogen), 3′ of the P10 promoter, and the polyhedron promoter (polh), respectively (pFastBac Dual/P10.OR/ polh.CYP2C9). Recombinant baculoviruses carrying both CYP2C9 and OR cDNAs were produced according to the Bac-to-Bac Baculovirus Expression system protocol of Invitrogen.

Expression of Recombinant Proteins in Insect Cells and Preparation of Microsomal Fractions

For the expression of recombinant proteins using the baculovirus expression systems, adherent *Spodoptera frugiperda* (*Sf21*) insect cells (3.7×10^8 cells per 225 cm^2 flask) were infected with recombinant baculoviruses at a multiplicity of infection of 4 in supplemented form of Grace's Insect Medium (Invitrogen) with 10% fetal bovine serum and 10 μg/mL gentamycin. At 16–24 h post-infection, the culture media were supplemented with 0.2 mmol/L ferric citrate and 0.3 mmol/L δ-aminolevulinic acid, and the cells were harvested at 72-h post-infection. Microsomal fractions from *Sf21* cells were prepared as described previously (*11*).

Characterization of Protein Expression

The cytochrome P450 content in insect cell microsomes was measured by reduced CO-spectrum using the method of Omura and Sato (*32*). NADPH-cytochrome P450 OR activity in insect cell microsomes was measured using cytochrome C as a substrate as described by Phillips and Langdon (*33*). The molar amount of OR was calculated based on an assumed specific activity of 3.0 μmol cytochrome C reduced/min/nmol purified human OR (*34*). Western blotting of CYP2C9 and OR was performed using 2 μg of microsomal protein from insect cells as described previously (*11*). For immunostaining of OR, goat anti-rat OR antiserum (diluted 1:1,000; Daiichi Pure Chemical Co., Tokyo, Japan) and horseradish peroxidase–conjugated rabbit anti-goat IgG (diluted 1:20,000; Jackson ImmunoResearch Laboratories, West Grove, USA) were used as the first and second antibodies, respectively.

Assay for CYP2C9-Mediated Enzymatic Activity

CYP2C9 activities for the wild-type and two variants were assessed by diclofenac 4′-hydroxylation as described previously (*11*) except that the incubation mixture contained diclofenac (1.0–100 μmol/L), 5 pmol of P450 from insect microsomes, 10 pmol of purified cytochrome b5 (Oxford Biomedical Research, Oxford, UK), and an NADPH regenerating system (1.3 mmol/L $NADP^+$, 3.3 mmol/L glucose 6-phosphate, 3.3 mmol/L $MgCl_2$ and 0.4 unit/mL glucose-6-phosphate dehydrogenase), and the reactions were allowed to proceed for 10 min. The initial mobile phase of high-performance liquid chromatography consisted of 70% of a 30% acetonitrile solution containing 1 mmol/L perchloric acid (A) and 30% of methanol (B) and was delivered for 5 min, after which a 20 min linear gradient from 30% to 100% of B was formed at a flow rate of 1 mL/min. Under these conditions, the retention times of 4′-hydroxydiclofenac, 5-hydroxydiclofenac, and diclofenac were 14.2, 14.7, and 19.6 min, respectively.

Table 1. Genetic Variants in *CYP2C9* Identified in 724 Japanese Individuals

SNP position[a]	SNP position[b]	Location	Nomenclature[c]	Amino acid change	Number of subjects			Minor allele frequency	Flanking sequences (5′ to 3′)	rs ID No.	Reference
					Wild-type	Heterozygote	Homozygote				
−251 C>A[d]	−251	promoter			723	1	0	0.0007	ttattaccaata[C>A]ctaggctccaac		
−162 A>G	−162	promoter			723	1	0	0.0007	cattttatttttt[A>G]tctgtatcagtg		(*27*)
251 T>C	IVS1 + 83	Intron 1			716	7	1	0.0062	cctagaggtaca[T>C]gttacaagaggt	rs9332104	
3136 T>C[d]	IVS1 − 40	Intron 1			722	2	0	0.0014	aaatggacaaaa[T>C]agtaacttcgtt		
3154 T>C	IVS1 − 22	Intron 1			723	1	0	0.0007	cttcgtttgctg[T>C]tatctctgtcta		(*11*)
3235 G>A	228	Exon 2		Val76	706	18	0	0.0124	acccatagtggt[G>A]ctgcatggatat	rs17847036	
3276 T>C	269	Exon 2	*CYP2C9*13*	Leu90Pro	722	2	0	0.0014	ccctgattgatc[T>C]tggagaggagtt		(*6*)
3411 T>C	IVS2 + 73	Intron 2			712	11	1	0.0090	gacttacagagc[T>C]cctcgggcagag	rs9332120	
3451 G>A[d]	IVS2 − 59	Intron 2			723	1	0	0.0007	tggctgcccagt[G>A]tcagcttcctct		
3455 G>C[d]	IVS2 − 55	Intron 2			723	1	0	0.0007	tgcccagtgtca[G>C]cttcctctttct		
3488 G>T[d]	IVS2 − 22	Intron 2			723	1	0	0.0007	atctccctccta[G>T]tttcgtttctctt		
3514 T>C	336	Exon 3		Ile112	721	3	0	0.0021	tgttaggaat[T>C]gttttcagca		(*11*)
3544 G>A[d]	366	Exon 3		Glu122	723	1	0	0.0007	gaaatggaagga[G>A]atccggcgtttc		
3552 G>A	374	Exon 3	*CYP2C9*14*	Arg125His	723	1	0	0.0007	aggagatccggc[G>A]tttctccctcat		(*7*)
3573 G>A[d]	395	Exon 3		Arg132Gln	723	1	0	0.0007	tcatgacgctgc[G>A]gaattttgggat		
3627 G>T	449	Exon 3	*CYP2C9*27*	Arg150Leu	721	3	0	0.0021	aagaggaagccc[G>T]ctgccttgtgga		(*11*)
9032 G>C	IVS3 − 65	Intron 3			592	126	6	0.0953	ctactattatct[G>C]ttaacaaataca	rs9332127	
10411 A>G[d]	IVS4 − 15	Intron 4			723	1	0	0.0007	atttaataaatt[A>G]ttgttttctctt		
33553 A>G[d]	951	Exon 6		Pro317	723	1	0	0.0007	gctgaagcaccc[A>G]gaggtcacaggt		
42543 G>A[d]	1004	Exon 7		Arg335Gln	722	2	0	0.0014	ttggcagaaacc[G>A]gagcccctgcat		
42614 A>C	1075	Exon 7	*CYP2C9*3*	Ile359Leu	677	47	0	0.0325	gtccagagatac[A>C]ttgaccttctcc	rs1057910	
42676 T>C	1137	Exon 7		Tyr379	714	10	0	0.0069	attcagaaacta[T>C]ctcattcccaag		(*11*)
47377 T>C[d]	1176	Exon 8		Thr392	723	1	0	0.0007	aatttccctgac[T>C]tctgtgctacat		
50298 A>T	1425	Exon 9		Gly475	678	46	0	0.0319	agttgtcaatgg[A>T]tttgcctctgtg	rs1057911	
50302 G>A	1429	Exon 9	*CYP2C9*30*	Ala477Thr	722	2	0	0.0014	gtcaatggattt[G>A]cctctgtgccgc		(*11*)
50369 C>T[d]	1496 (*23[e])	3′-UTR			723	1	0	0.0007	atggcctggctg[C>T]tgctgtgcagtc		
50378 A>G[d]	1505 (*32[e])	3′-UTR			722	2	0	0.0014	ctgctgctgtgc[A>G]gtccctgcagct		
50456 C>T[d]	1583 (*110[e])	3′-UTR			721	3	0	0.0021	cctgtcatctca[C>T]attttcccttcc		
50613 T>C[d]	1740 (*267[e])	3′-UTR			722	2	0	0.0014	ttgagttattaa[T>C]atgttattatta		
50614 AT>—	1741_1742 (*268_*269[e])	3′-UTR			721	3	0	0.0021	tgagttattaat[AT>—]gttattattaaa		(*7*)
50742 T>A	1835+34[f] (*396[e])	3′ flanking			686	38	0	0.0263	ttcttttatgca[T>A]aatgtaggtcag	rs9332245	

[a]The A of the ATG of the initiation Met codon is denoted as nucleotide + 1. [b]From the translational initiation site or from the end of the nearest exon. [c]Nomenclature for *CYP2C9* allele cited from: http://www.cypalleles.ki.se/cyp2c9.htm [d]Novel mutations identified in this study. [e]The nucleotide following the translation termination codon TGA is numbered *1. [f]The first nucleotide downstream of the 3′-end of exon 9 is numbered + 1.

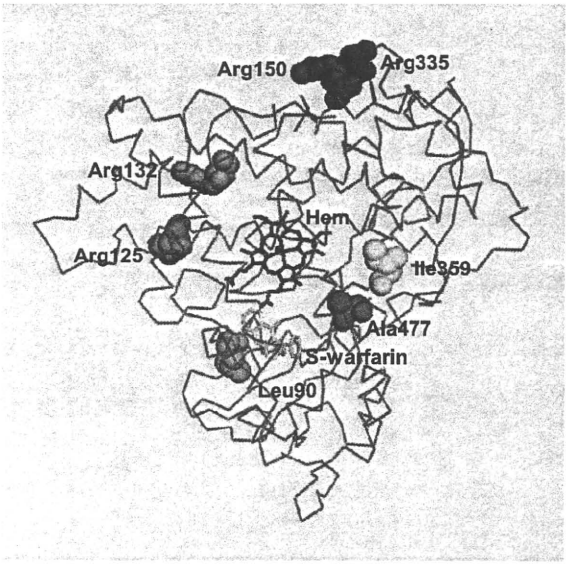

Fig. 1. *Mapping of identified missense variations on the crystal structure of human CYP2C9 protein bound with warfarin (PDB: 10G5). Hem and S-warfarin are shown by red and pink, respectively. The seven missense mutations identified in this study are presented by a space-filling model.*

Statistical Analysis

All SNPs identified were tested for deviations from the Hardy-Weinberg disequilibrium through the use of a χ^2 test. Pairwise linkage disequilibrium (LD) between two SNPs was evaluated by r^2 using SNPAlyze version 4.0 software (DYNACOM Co., Ltd., Mobara, Japan). Kinetic parameters K_m and V_{max} were estimated using a software program designed for non-linear regression analysis of a hyperbolic Michaelis-Menten equation (Prism v.3.0a, GraphPad Software, San Diego, USA). Kinetic data are presented as the mean±SD for three microsomal preparations derived from separate transfections for each variant and analyzed by one-way analysis of variance. Multiple comparisons were made with the Scheffe test.

Results

Resequence of *CYP2C9* in 724 Japanese Subjects

Upon sequencing the *CYP2C9* in 724 Japanese subjects, we identified a total of 31 genetic variations, including 15 novel ones (Table 1). All of the detected variations (except for the SNPs of 251 C>A in intron 1 and 3411 T>C in intron 2) were in Hardy-Weinberg equilibrium for two separate groups ($p \geq 0.81$ in stroke patients and $p \geq 0.82$ in hypertensive patients) and for all subjects ($p \geq 0.66$). Since we did not find any significant differences in frequencies between the stroke patients and the hypertensive patients ($p > 0.05$ by χ^2 test or Fisher's exact test), the data for all subjects were analyzed as one group.

Fourteen variations (seven missense and seven synonymous ones) were identified in the coding regions of CYP2C9. Two out of the seven missense mutations were novel, including Arg132Gln in one hypertensive patient and Arg335Gln in two stroke patients. The other five known missense mutations, Ile359Leu (*CYP2C9*3*), Leu90Pro (*CYP2C9*13*), Arg125His (*CYP2C9*14*), Arg150Leu (*CYP2C9*27*), and Ala447Thr (*CYP2C9*30*), were found in 47, 2, 1, 3, and 2 individuals, respectively. All the missense mutations were heterozygous, and there were no compound heterozygotes. The positions of seven missense mutations on the crystal structure of human CYP2C9 bound with warfarin are shown in Fig. 1.

Seven synonymous variations were identified, of which three novel ones (Glu122Glu; $n=1$, Pro317Pro; $n=1$, and Thr392Thr; $n=1$) were found as single heterozygotes. In the putative promoter region, two variants (−251 C>A and −162 A>G) (*35*) were detected, each in only one individual. A total of 15 variations were found in the intronic, 3′-UTR, and 3′-flanking regions. Five novel variations in introns 1, 2, and 4 and four novel variations in the 3′-UTR were identified with allele frequencies less than 0.01.

LD analysis showed that *CYP2C9*3* was in LD ($r^2 > 0.8$) with two variations, 50298 A>T (Gly475Gly) in exon 9 and 50742 T>A in the 3′-flanking region. LD ($r^2 = 0.7$) was also noted between two intronic variants, 251 T>C in intron 1 and 3411 T>C in intron 2.

Functional Characterization of Two Novel Missense Mutations

To functionally characterize the two novel missense mutations, Arg132Gln and Arg335Gln, the wild-type and two CYP2C9 variants were coexpressed with NADPH-cytochrome P450 OR in *Sf21* insect cells. The holo-CYP2C9 content was not significantly different between the wild-type and variants: 188.6±22.9 pmol/mg microsomal protein for wild-type, 192.3±14.5 pmol/mg microsomal protein for Arg132Gln, and 159.3±5.5 pmol/mg microsomal protein for Arg335Gln, as determined on three lots from independent expression experiments. Quantities of cytochrome P420 were negligible for all preparations (data not shown). Cytochrome C reductase activities varied slightly but were not significantly different among the preparations (632–808 nmol cytochrome C reduced/min/mg protein), and the mean OR/CYP2C9 molar ratios in microsomal fractions were calculated to be 1.2, 1.3, and 1.6 for wild-type, Arg132Gln, and Arg335Gln, respectively.

Immunoblot analyses of CYP2C9 and OR were performed using insect cell microsomes, and representative data from three independent preparations are shown in Fig. 2. Quantitative analysis revealed that neither apo-CYP2C9 nor OR pro-

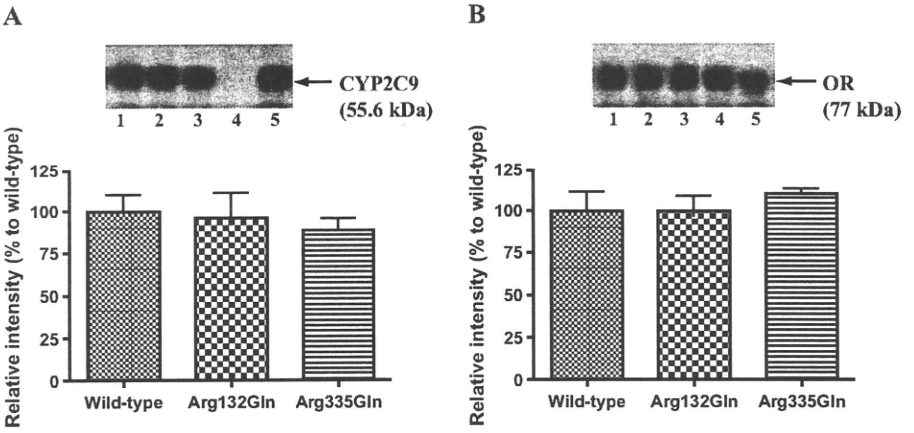

Fig. 2. *Expression of wild-type and two variants of CYP2C9 in insect cell microsomes. Representative Western blots of immunoreactive CYP2C9 (A) and OR (B) proteins (upper) are shown. Lanes 1–3: co-expressed microsomes containing wild-type, Arg132Gln, and Arg335Gln CYP2C9 each with OR; lane 4: microsomes containing solely OR; lane 5: commercially available co-expressed supersomes containing CYP2C9.1 and OR (BD Bioscience, San Jose, USA). Relative intensities of immunoreactive CYP2C9 (A) and OR (B) protein are shown in the lower panels. Each bar represents the mean±SD of three separate experiments.*

Table 2. Kinetic Parameters for Hydroxylation Activities of Wild-Type and Variant CYP2C9 against Diclofenac

Amino acid alteration	K_m (μmol/L)	V_{max} (pmol/min/pmol P450)	Clearance (V_{max}/K_m) (μL/min/pmol P450)
Wild-type	3.4±0.17	79.8±6.6	23.4±0.81
Arg132Gln	1.8±0.05**	7.8±0.4**	4.2±0.31**
Arg335Gln	3.0±0.10*	65.4±2.1*	22.0±0.06*

*$p<0.05$, **$p<0.0001$ *vs.* wild-type. One-way analysis of variance, post-hoc test: Scheffe. Data are represented by means±SD.

tein expression levels were significantly different among the wild-type and two variants ($p=0.77$ for CYP2C9, $p=0.64$ for OR). Catalytic activities of the wild-type and variant (Arg132Gln and Arg335Gln) proteins were assessed using diclofenac as a substrate. Diclofenac 4′-hydroxylation exhibited typical hyperbolic kinetic profiles in both the wild-type and variant proteins (data not shown). The kinetic parameters are summarized in Table 2. The Arg132Gln protein showed a 90% decrease in the V_{max} value and a partial decrease in the K_m value, resulting in fivefold lower intrinsic clearance relative to the wild-type (Table 2). A slight diminution in intrinsic clearance (6%) was observed for the Arg335Gln protein with slightly decreased K_m and V_{max} values (Table 2). The formation of 5-hydroxy diclofenac was observed in neither the wild-type nor variant (Arg132Gln and Arg335Gln) proteins (data not shown), suggesting that these substitutions do not alter the regioselectivity of diclofenac hydroxylation.

CYP2C9 Polymorphisms and the Effectiveness of Losartan in 39 Hypertensive Patients

Among 39 patients taking losartan, 34 patients carried the wild genotype of *CYP2C9*1/*1*, and the other 5 patients carried missense mutations, including *CYP2C9*1/*3* in 2 patients, *CYP2C9*1/*30* in 2 patients, and Arg132Gln mutation in one patient. The changes in systolic and diastolic blood pressure with respect to genotypes at 3 months of losartan treatment are presented in Table 3. Losartan obviously lowered systolic blood pressure in 2 patients with *CYP2C9*3* and in a patient with the Arg132Gln mutation. However, losartan was not effective in 2 patients with *CYP2C9*1/*30*.

Discussion

In the present study, the large-scale direct resequencing effort of the *CYP2C9* allowed us to detect 31 genetic variations in 724 Japanese individuals. We also obtained accurate frequencies of the known variations, *CYP2C9*3*, **13*, **14*, **27* and **30*, that are specific to Asians, except for **3*. As for the novel alleles, Arg132Gln and Arg335Gln, their effects on both protein expression levels and enzymatic activity were assessed using a baculovirus expression system.

The most frequently identified missense mutation in the present study was *CYP2C9*3* (Ile359Leu), with a frequency

Table 3. Patient Characteristics and Blood Pressure Response to Losartan with Respect to Genotypes: Essential Hypertensive Patients Taking Losartan

	CYP2C9 genotype					
	**1/*1*	**1/*3*		**1/*30*		Arg132Gln
Case number	34	2		2		1
Sex (male/female)	21/13	0/2		2/0		1/0
Age (years)	65.10±7.04	70	67	77	71	70
BMI (kg/m^2)	25.10±3.07	21.47	24.20	24.33	25.59	20.7
SBP						
At baseline (mmHg)	151.10±14.75	130[a]	156	155	172	157
At 3 month (mmHg)	142.80±16.23	119	141	151	173	128
Change (mmHg)	−8.70±14.35	−11	−15	−4	1	−29
DBP						
At baseline (mmHg)	88.80±9.26	71[a]	104	81	98	82
At 3 month (mmHg)	84.90±9.98	75	96	83	95	70
Change (mmHg)	−4.20±6.91	4	−8	2	−3	−12

Values are mean±SD. BMI, body mass index; SBP, DBP, systolic and diastolic blood pressures. [a]Office blood pressure in this patient with *CYP2C9 *1/*3* was 130/71 mmHg. Losartan was prescribed because this patient had higher home SBP (over 150 mmHg).

of 0.033, which was in good agreement with the previously published results in Japanese populations (*11*, *36*, *37*). The frequency of *CYP2C9*13* (Leu90Pro), 0.0014 in the present study, was comparable to that recently reported in a Japanese population (*11*) but much lower than those in previous studies of other Asian populations (*6*, *9*). *CYP2C9*13* was first identified in a Chinese individual who showed poor metabolizer phenotype for both lornoxicam and tolbutamide (*6*). Functional analysis of the *CYP2C9*13* protein showed decreased enzymatic activity for tolbutamide and diclofenac (*10*). Another recently published allele, *CYP2C9*14* (Arg125His), was detected in an individual in the present study. This allele was first identified in an Indian patient, and the variant protein exhibited 80–90% lower catalytic activity toward tolbutamide (*7*, *8*). *CYP2C9*27* (Arg150Leu) and **30* (Ala477Thr), both detected recently in a Japanese population (*11*), were also identified in 3 and 2 individuals in the present study, respectively. The *in vitro* study revealed that the *CYP2C9*30* protein had a twofold higher K_m value and a threefold lower V_{max} value than the wild-type towards diclofenac, whereas the catalytic activity of the *CYP2C9*27* protein was similar to the wild-type (*11*).

The novel Arg132Gln variant exhibited a 90% decrease in the V_{max} value toward diclofenac 4′-hydroxylation (Table 2). Arg132 is located in a loop region between the C and D helices (Fig. 1) and is highly conserved in the CYP2C family (http://drnelson.utmem.edu/humP450.aln.html). Arg133, the corresponding residue of CYP2B4, is suggested to play a prominent role in binding its redox partners, cytochrome b5 and P450 reductase (*38*). Accordingly, the loss of catalytic activity of the Arg132Gln variant might reflect the altered affinity of variant protein to these redox partners due to electrostatic changes as proposed for **2* (Arg144Cys), **14* (Arg125His), and **26* (Thr130Arg) (*8*, *11*, *39*).

The Arg335Gln variant showed a similar holo-CYP2C9 content to wild-type in insect cell microsomes. Furthermore, the intrinsic clearance of the Arg335Gln variant was only slightly lower than that of the wild-type. In contrast to Arg335Gln, a substitution in the same position, Arg335Trp (**11*), was reported to exhibit a threefold increase in K_m and more than a twofold decrease in the intrinsic clearance for tolbutamide when expressed in a bacterial cDNA expression system (*40*). In addition, catalytically active *CYP2C9*11* holo protein was expressed at a very low level due to its decreased stability in insect cells (*41*). To confirm whether or not the protein stability of the Arg335Gln variant might be influenced by the *in vitro* expression system used, the wild-type and variant proteins were expressed in a mammalian expression system using COS-1 cells. The protein expression level of Arg335Gln variant in COS-1 microsomes was decreased by only 30% compared with that of the wild-type (data not shown), indicating that the protein stability of the Arg335Gln product was not substantially different between mammalian expression systems and baculovirus/insect cell systems. Thus, the substituted residues (Trp *vs.* Gln) at this position might quite differently influence the stability of protein as well as catalytic activities.

Thirty-nine patients were taking losartan, which is known to exhibit considerable inter-individual variation in its antihypertensive effects. Losartan is primarily oxidized by CYP2C9 to an active carboxylic acid metabolite, E-3174 (*14–16*). CYP3A4 also plays a limited role in the metabolic activation of losartan *in vitro*; however, its significance *in vivo* has not been demonstrated (*3*, *15*, *16*). We evaluated the impact of *CYP2C9* variations on the antihypertensive effect of losartan based on the patients' average resting blood pressure measured before and three months after losartan treatment.

Two Japanese hypertensive patients carrying the *CYP2C9*3* heterozygous allele showed lowered systolic blood pressure by losartan (Table 3). This is in line with the previous report that no significant differences in the pharmacokinetics of losartan and E-3174 were observed between *CYP2C9*1/*3* and **1/*1* (*42*). Contrary to our result, a Danish prospective study of optimal monotherapy with losartan in type 1 diabetic patients with nephropathy showed that the reduction in systolic 24 h blood pressure was significantly greater in wild-type patients (n=48) than in *CYP2C9*3* carriers (n=12) (*43*). Furthermore, similar changes in diastolic and systolic 12 h blood pressures were also observed between *CYP2C9*1/*1* (n=4) and **1/*3* (n=3) Japanese patients (*20*). The role of heterozygous *CYP2C9*3* in the blood pressure–lowering response to losartan in hypertensive patients should be further studied in a large cohort of patients.

Inconsistent with our *in vitro* study, systolic blood pressure in a patient with Arg132Gln was obviously lowered by losartan (Table 3). For this variation, the substrate-dependent differences between diclofenac and losartan oxidation are unlikely because Arg132 might interact with redox partners but not with substrates as described above. However, the change in enzymatic activity toward losartan should be further analyzed.

However, losartan was not effective in 2 patients carrying the heterozygous *CYP2C9*30* (Ala477Thr) allele. A serious impact on the pharmacodynamics of losartan was not demonstrated statistically because of the small sample size of individuals with **30*. Ala477 is located in the substrate recognition site-6 region in the β2 sheet, which shows very strong hydrophobic interactions with the substrates (*44*), suggesting the importance of this residue in metabolic activity of CYP2C9 toward various substrates. Therefore, insufficient conversion of losartan to E-3174 by this defective mutation might be responsible for the therapeutic failure of these patients. Pharmacokinetic analysis of *CYP2C9*30* towards losartan would be necessary to further elucidate its clinical relevance.

In conclusion, multiple rare functional variations of *CYP2C9* were detected in a Japanese population. Approximately 7% of the Japanese individuals analyzed (53 of 724) carried one of the functionally deleterious alleles (*CYP2C9*3*, **13*, **14*, **30*, and Arg132Gln). In addition to *CYP2C9*3*, *CYP2C9*30* might also be used for determining inter-individual responses to losartan treatment in Japanese hypertensive patients.

Acknowledgements

We thank Ms. Junko Ishikawa and Mr. Katsuhiro Yamamoto of the National Cardiovascular Center for their technical assistance.

References

1. Miners JO, Birkett DJ: Cytochrome P4502C9: an enzyme of major importance in human drug metabolism. *Br J Clin Pharmacol* 1998; **45**: 525–538.
2. Evans WE, Relling MV: Pharmacogenomics: translating functional genomics into rational therapeutics. *Science* 1999; **286**: 487–491.
3. Lee CR, Goldstein JA, Pieper JA: Cytochrome P450 2C9 polymorphisms: a comprehensive review of the *in-vitro* and human data. *Pharmacogenetics* 2002; **12**: 251–263.
4. Kirchheiner J, Brockmoller J: Clinical consequences of cytochrome P450 2C9 polymorphisms. *Clin Pharmacol Ther* 2005; **77**: 1–16.
5. Schwarz UI: Clinical relevance of genetic polymorphisms in the human CYP2C9 gene. *Eur J Clin Invest* 2003; **33** (Suppl 2): 23–30.
6. Si D, Guo Y, Zhang Y, *et al*: Identification of a novel variant CYP2C9 allele in Chinese. *Pharmacogenetics* 2004; **14**: 465–469.
7. Zhao F, Loke C, Rankin SC, *et al*: Novel CYP2C9 genetic variants in Asian subjects and their influence on maintenance warfarin dose. *Clin Pharmacol Ther* 2004; **76**: 210–219.
8. DeLozier TC, Lee SC, Coulter SJ, *et al*: Functional characterization of novel allelic variants of CYP2C9 recently discovered in southeast Asians. *J Pharmacol Exp Ther* 2005; **315**: 1085–1090.
9. Bae JW, Kim HK, Kim JH, *et al*: Allele and genotype frequencies of CYP2C9 in a Korean population. *Br J Clin Pharmacol* 2005; **60**: 418–422.
10. Guo Y, Zhang Y, Wang Y, *et al*: Role of CYP2C9 and its variants (CYP2C9*3 and CYP2C9*13) in the metabolism of lornoxicam in humans. *Drug Metab Dispos* 2005; **33**: 749–753.
11. Maekawa K, Fukushima-Uesaka H, Tohkin M, *et al*: Four novel defective alleles and comprehensive haplotype analysis of CYP2C9 in Japanese. *Pharmacogenet Genomics* 2006; **16**: 497–514.
12. Dahlof B, Devereux RB, Kjeldsen SE, *et al*: Cardiovascular morbidity and mortality in the Losartan Intervention For Endpoint reduction in hypertension study (LIFE): a randomised trial against atenolol. *Lancet* 2002; **359**: 995–1003.
13. Baudin B: Angiotensin II receptor polymorphisms in hypertension. Pharmacogenomic considerations. *Pharmacogenomics* 2002; **3**: 65–73.
14. Lo MW, Goldberg MR, McCrea JB, *et al*: Pharmacokinetics of losartan, an angiotensin II receptor antagonist, and its active metabolite EXP3174 in humans. *Clin Pharmacol Ther* 1995; **58**: 641–649.
15. Stearns RA, Chakravarty PK, Chen R, Chiu SH: Biotransformation of losartan to its active carboxylic acid metabolite in human liver microsomes. Role of cytochrome P4502C and 3A subfamily members. *Drug Metab Dispos* 1995; **23**: 207–215.
16. Yasar U, Tybring G, Hidestrand M, *et al*: Role of CYP2C9 polymorphism in losartan oxidation. *Drug Metab Dispos* 2001; **29**: 1051–1056.
17. Yasar U, Forslund-Bergengren C, Tybring G, *et al*: Pharmacokinetics of losartan and its metabolite E-3174 in relation to the CYP2C9 genotype. *Clin Pharmacol Ther* 2002; **71**: 89–98.
18. Yasar U, Dahl ML, Christensen M, Eliasson E: Intra-indi-

vidual variability in urinary losartan oxidation ratio, an *in vivo* marker of CYP2C9 activity. *Br J Clin Pharmacol* 2002; **54**: 183–185.

19. Babaoglu MO, Yasar U, Sandberg M, *et al*: CYP2C9 genetic variants and losartan oxidation in a Turkish population. *Eur J Clin Pharmacol* 2004; **60**: 337–342.
20. Sekino K, Kubota T, Okada Y, *et al*: Effect of the single CYP2C9*3 allele on pharmacokinetics and pharmacodynamics of losartan in healthy Japanese subjects. *Eur J Clin Pharmacol* 2003; **59**: 589–592.
21. Matayoshi T, Kamide K, Takiuchi S, *et al*: The thiazide-sensitive Na^{+}-Cl^{-} cotransporter gene, C1784T, and adrenergic receptor-β3 gene, T727C, may be gene polymorphisms susceptible to the antihypertensive effect of thiazide diuretics. *Hypertens Res* 2004; **27**: 821–833.
22. Kimura R, Miyashita K, Kokubo Y, *et al*: Genotypes of vitamin K epoxide reductase, γ-glutamyl carboxylase, and cytochrome P450 2C9 as determinants of daily warfarin dose in Japanese patients. *Thromb Res* 2007; **120**: 181–186.
23. Kamide K, Tanaka C, Takiuchi S, *et al*: Six missense mutations of the epithelial sodium channel β and γ subunits in Japanese hypertensives. *Hypertens Res* 2004; **27**: 333–338.
24. Kamide K, Takiuchi S, Tanaka C, *et al*: Three novel missense mutations of WNK4, a kinase mutated in inherited hypertension, in Japanese hypertensives: implication of clinical phenotypes. *Am J Hypertens* 2004; **17**: 446–449.
25. Kamide K, Yang J, Kokubo Y, *et al*: A novel missense mutation, F826Y, in the mineralocorticoid receptor gene in Japanese hypertensives: its implications for clinical phenotypes. *Hypertens Res* 2005; **28**: 703–709.
26. Kamide K, Kokubo Y, Hanada H, *et al*: Genetic variations of *HSD11B2* in hypertensive patients and in the general population, six rare missense/frameshift mutations. *Hypertens Res* 2006; **29**: 243–252.
27. Kimura R, Kokubo Y, Miyashita K, *et al*: Polymorphisms in vitamin K–dependent γ-carboxylation–related genes influence interindividual variability in plasma protein C and protein S activities in the general population. *Int J Hematol* 2006; **84**: 387–397.
28. Yin T, Hanada H, Miyashita K, *et al*: No association between vitamin K epoxide reductase complex subunit 1–like 1 (VKORC1L1) and the variability of warfarin dose requirement in a Japanese patient population. *Thromb Res* 2008; **122**: 179–184.
29. Banno M, Hanada H, Kamide K, *et al*: Association of genetic polymorphisms of endothelin-converting enzyme-1 gene with hypertension in a Japanese population and rare missense mutation in preproendothelin-1 in Japanese hypertensives. *Hypertens Res* 2007; **30**: 513–520.
30. Kokame K, Matsumoto M, Soejima K, *et al*: Mutations and common polymorphisms in ADAMTS13 gene responsible for von Willebrand factor–cleaving protease activity. *Proc Natl Acad Sci U S A* 2002; **99**: 11902–11907.
31. Williams PA, Cosme J, Ward A, *et al*: Crystal structure of human cytochrome P450 2C9 with bound warfarin. *Nature* 2003; **424**: 464–468.
32. Omura T, Sato R: The carbon monoxide–binding pigment of liver microsomes. I. Evidence for its hemoprotein nature. *J Biol Chem* 1964; **239**: 2370–2378.
33. Phillips AH, Langdon RG: Hepatic triphosphopyridine nucleotide-cytochrome c reductase: isolation, characterization, and kinetic studies. *J Biol Chem* 1962; **237**: 2652–2660.
34. Yamazaki H, Nakajima M, Nakamura M, *et al*: Enhancement of cytochrome P-450 3A4 catalytic activities by cytochrome b5 in bacterial membranes. *Drug Metab Dispos* 1999; **27**: 999–1004.
35. Shintani M, Ieiri I, Inoue K, *et al*: Genetic polymorphisms and functional characterization of the 5′-flanking region of the human CYP2C9 gene: *in vitro* and *in vivo* studies. *Clin Pharmacol Ther* 2001; **70**: 175–182.
36. Nasu K, Kubota T, Ishizaki T: Genetic analysis of CYP2C9 polymorphism in a Japanese population. *Pharmacogenetics* 1997; **7**: 405–409.
37. Yin T, Miyata T: Warfarin dose and the pharmacogenomics of CYP2C9 and VKORC1-rationale and perspectives. *Thromb Res* 2007; **120**: 1–10.
38. Bridges A, Gruenke L, Chang YT, *et al*: Identification of the binding site on cytochrome P450 2B4 for cytochrome b5 and cytochrome P450 reductase. *J Biol Chem* 1998; **273**: 17036–17049.
39. Crespi CL, Miller VP: The R144C change in the CYP2C9*2 allele alters interaction of the cytochrome P450 with NADPH: cytochrome P450 oxidoreductase. *Pharmacogenetics* 1997; **7**: 203–210.
40. Blaisdell J, Jorge-Nebert LF, Coulter S, *et al*: Discovery of new potentially defective alleles of human CYP2C9. *Pharmacogenetics* 2004; **14**: 527–537.
41. Tai G, Farin F, Rieder MJ, *et al*: *In-vitro* and *in-vivo* effects of the CYP2C9*11 polymorphism on warfarin metabolism and dose. *Pharmacogenet Genomics* 2005; **15**: 475–481.
42. Lee CR, Pieper JA, Hinderliter AL, Blaisdell JA, Goldstein JA: Losartan and E3174 pharmacokinetics in cytochrome P450 2C9*1/*1, *1/*2, and *1/*3 individuals. *Pharmacotherapy* 2003; **23**: 720–725.
43. Lajer M, Tarnow L, Andersen S, Parving HH: CYP2C9 variant modifies blood pressure–lowering response to losartan in Type 1 diabetic patients with nephropathy. *Diabet Med* 2007; **24**: 323–325.
44. Afzelius L, Zamora I, Ridderstrom M, Andersson TB, Karlen A, Masimirembwa CM: Competitive CYP2C9 inhibitors: enzyme inhibition studies, protein homology modeling, and three-dimensional quantitative structure-activity relationship analysis. *Mol Pharmacol* 2001; **59**: 909–919.

21 Angleton P, Chandler WL, Schmer G. Diurnal variation of tissue-type plasminogen activator and its rapid inhibitor (PAI-1). *Circulation* 1989; **79**: 101–6.
22 Muller JE, Stone PH, Turi ZG, Rutherford JD, Czeisler CA, Parker C, Poole WK, Passamani E, Roberts R, Robertson T, Sobel BE, Willerson JT, Braunwauld E, the MILIS Study Group. Circadian variation in the frequency of onset of acute myocardial infarction. *N Engl J Med* 1985; **313**: 1315–22.
23 Marler JR, Price TR, Clark GL, Muller JE, Robertson T, Mohr JP, Hier DB, Wolf PA, Caplan LR, Foulkes MA. Morning increase in onset of ischemic stroke. *Stroke* 1989; **20**: 473–6.

ADAMTS13 P475S polymorphism causes a lowered enzymatic activity and urea lability *in vitro*

M. AKIYAMA, K. KOKAME and T. MIYATA
National Cardiovascular Center Research Institute, Osaka, Japan

To cite this article: Akiyama M, Kokame K, Miyata T. ADAMTS13 P475S polymorphism causes a lowered enzymatic activity and urea lability *in vitro*. *J Thromb Haemost* 2008; **6**: 1830–2.

von Willebrand factor (VWF) is a plasma glycoprotein synthesized primarily in vascular endothelial cells and megakaryocytes [1]. VWF is released into plasma as ultra-large multimeric forms that are highly active in platelet aggregation. A plasma metalloprotease ADAMTS13 specifically cleaves the Tyr^{1605}-Met^{1606} peptidyl bond within the A2 domain of VWF [2]. Deficiency of the ADAMTS13 enzymatic activity, caused by genetic mutations or acquired autoantibodies against ADAMTS13, results in the accumulation of ultra-large VWF multimers in plasma that lead to the hyper-aggregation of platelets. This prothrombotic condition can cause thrombotic thrombocytopenic purpura (TTP) [3]. A number of non-synonymous mutations and polymorphisms of ADAMTS13 have been identified [4,5]. Among them, the P475S (c.1423C > T) polymorphism is noteworthy.

The allele frequency of ADAMTS13 P475S was 5.1% in Japanese subjects [6], 4.0% in Koreans [7], and 1.5% in Chinese [8], but absent in Caucasians [9]. The recombinant P475S mutant was normally secreted from cultured cells but showed greatly reduced enzymatic activity (~10%) in the VWF-multimer assay [6]. Recently, we have developed a quantitative ADAMTS13 activity assay using a synthetic fluorogenic substrate FRETS-VWF73 [10] and it is now widely utilized [11–14]. The assay can be performed in the absence of urea that is required for the VWF-multimer assay. In this study, we evaluated the activity of the P475S mutant using FRETS-VWF73 and found that the mutant exhibited the more profound loss of activity than the wild-type in the presence of urea.

Correspondence: Koichi Kokame, National Cardiovascular Center Research Institute, 5-7-1 Fujishirodai, Suita, Osaka 565-8565, Japan.
Tel.: +81 6 6833 5012 ext. 2460; fax: +81 6 6835 1176.
E-mail: kame@ri.ncvc.go.jp

DOI: 10.1111/j.1538-7836.2008.03109.x

Received 11 July 2008, accepted 18 July 2008

We have prepared four forms of recombinant ADAMTS13 using a transient expression system of HeLa cells: the full-length form (Met^{1}-Thr^{1427}) with the wild-type sequence (FL) or with the P475S polymorphism (FL-P475S), and the C-terminally-truncated forms (Met^{1}-Ala^{685}) with the wild-type sequence (MDTCS) or with the P475S polymorphism (MDTCS-P475S). FL and FL-P475S were tagged by the C-terminal FLAG sequence. MDTCS and MDTCS-P475S were tagged by the C-terminal 6xHis sequence. The culture media of cells expressing FL and FL-P475S were collected and concentrated 5-fold by centrifugal filtration (Ultrafree-MC; Millipore, Billerica, MA, USA). The media of cells expressing MDTCS and MDTCS-P475S were collected, and the recombinant proteins were purified by the Ni-NTA column chromatography. The relative amounts of the recombinant proteins were adjusted by their band intensities of Western blotting analysis using anti-FLAG or anti-6xHis antibodies, within the linear detection range. Enzymatic activity of each protein was measured by the FRETS-VWF73 assay [10] in the absence or presence of urea.

First, we compared the enzymatic activities between FL and FL-P475S in the absence of urea, and found that FL-P475S showed 71 ± 3.6% (n = 3) activity of FL. We previously reported that FL-P475S showed only approximately 10% activity of FL in the VWF-multimer assay [6]. This paradoxical observation led us to further study in order to understand the effect of P475S. We hypothesized that 1.5-M urea in the VWF-multimer assay [15] may affect the FL-P475S activity more severely than FL. Then, we added a series concentration of urea up to 2 M (final concentration) in the FRETS-VWF73 assay and measured the activity. Addition of urea inhibited the enzymatic activity of FL-P475S more severely than that of FL.

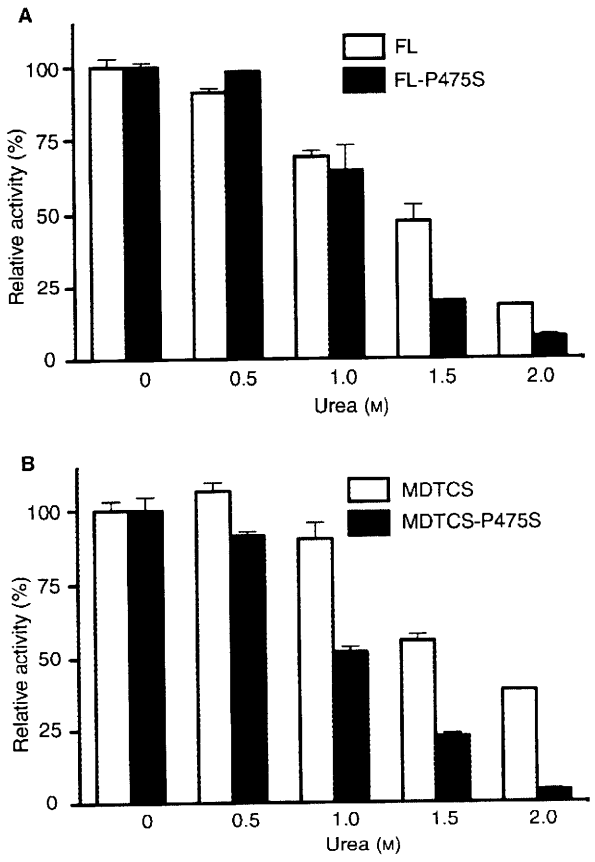

Fig. 1. Inhibitory effect of urea on the ADAMTS13 activity. (A) The enzymatic activities of recombinant full-length (FL, open bars) and its P475S mutant (FL-P475S, closed bars) were measured by the FRETS-VWF73 assay in the presence of urea at the indicated concentrations. FL-P475S showed 71% activity of FL in the absence of urea. The respective activities of FL and FL-P475S in the absence of urea were represented as 100%. Values are shown as mean with error bars indicating range (n = 2–3). (B) The enzymatic activities of C-terminally-truncated ADAMTS13 (MDTCS, open bars) and its P475S mutant (MDTCS-P475S, closed bars) were measured by the FRETS-VWF73 assay. MDTCS-P475S showed 66% activity of MDTCS in the absence of urea. The respective activities of MDTCS and MDTCS-P475S in the absence of urea were represented as 100%. Values are shown as mean with error bars indicating range (n = 3).

Compared with the urea-free condition, 1.5-M urea lowered the activities of FL and FL-P475S to 46% and 20%, respectively (Fig. 1A). Thus, it was suggested that FL-P475S showed 71% activity of FL in the absence of urea and 31% in the presence of 1.5-M urea.

To confirm the above results, we next compared the activities of purified recombinant MDTCS and MDTCS-P475S. MDTCS-P475S showed 66 ± 3.8% (n = 3) activity of MDTCS in the absence of urea. Urea again inhibited the activity of MDTCS-P475S more severely than that of MDTCS. Compared with the urea-free condition, 1.5-M urea lowered the activities of MDTCS and MDTCS-P475S to 55% and 22%, respectively (Fig. 1B). Thus, it was suggested that MDTCS-P475S showed 66% activity of MDTCS in the absence of urea, and 26% in the presence of 1.5-M urea. This was consistent with the data of FL and FL-P475S described above.

In the present study, we showed that P475S polymorphism of ADAMTS13 resulted in moderately lowered activity (~70%) in the FRETS-VWF73 assay without urea, and that the P475S mutant was more labile to urea than the wild-type. These results suggested that the greatly reduced activity of P475S mutant in the VWF-multimer assay (~10%) was partly explained by combined effects of the intrinsic lowered specific activity and lability to urea. In the VWF-multimer assay, denaturants such as urea must be present in the reaction buffer for efficient proteolysis of VWF by ADAMTS13. It is believed that urea can unravel the molecular conformation of VWF, resulting in exposing the scissile bond in the VWF A2 domain. At the same time, urea may partially disrupt the conformation of ADAMTS13. Substitution of Ser for Pro^{475} may enhance the denaturant effect of urea against ADAMTS13.

It is estimated that approximately 10% and 0.25% of the Japanese population are heterozygous or homozygous for P475S, respectively [6]. The frequency of hereditary TTP, however, is not so high in Japan [16], and no homozygotes of P475S have been so far identified as patients with hereditary TTP. Although P475S causes the lowered ADAMTS13 activity, the resultant activity seems sufficient for prevention of TTP onset. Further study will be needed for understanding the potential implication of P475S for acquired TTP or other thrombotic diseases.

Acknowledgements

This work was supported in part by the Program for Promotion of Fundamental Studies in Health Sciences of the National Institute of Biomedical Innovation (NIBIO) of Japan, grants-in-aid from the Ministry of Health, Labor, and Welfare of Japan, and grants-in-aid from the Ministry of Education, Culture, Sports, Science, and Technology of Japan.

Disclosure of Conflict of Interests

The authors state that they have no conflict of interest.

References

1 Sadler JE. Biochemistry and genetics of von Willebrand factor. *Annu Rev Biochem* 1998; **67**: 395–424.
2 Dent JA, Galbusera M, Ruggeri ZM. Heterogeneity of plasma von Willebrand factor multimers resulting from proteolysis of the constituent subunit. *J Clin Invest* 1991; **88**: 774–82.
3 Sadler JE, Moake JL, Miyata T, George JN. Recent advances in thrombotic thrombocytopenic purpura. *Hematology Am Soc Hematol Educ Program* 2004; 407–23.
4 Kokame K, Miyata T. Genetic defects leading to hereditary thrombotic thrombocytopenic purpura. *Semin Hematol* 2004; **41**: 34–40.
5 Banno F, Miyata T. Biology of an antithrombotic factor – ADAMTS13. In: Tanaka K, Davie EW, eds. *Recent Advances in Thrombosis and Hemostasis 2008*. Berlin: Springer, 2008: 162–76.

6 Kokame K, Matsumoto M, Soejima K, Yagi H, Ishizashi H, Funato M, Tamai H, Konno M, Kamide K, Kawano Y, Miyata T, Fujimura Y. Mutations and common polymorphisms in ADAMTS13 gene responsible for von Willebrand factor-cleaving protease activity. *Proc Natl Acad Sci U S A* 2002; **99**: 11902–7.
7 Jang MJ, Kim NK, Chong SY, Kim HJ, Lee SJ, Kang MS, Oh D. Frequency of Pro475Ser polymorphism of ADAMTS13 gene and its association with ADAMTS-13 activity in the Korean population. *Yonsei Med J* 2008; **49**: 405–8.
8 Gao W, Dai L, Su J, Wang Z, Ruan C. The frequency of P475S polymorphism in von Willebrand factor-cleaving protease in the Chinese population and its relevance to arterial thrombotic disorders. *Thromb Haemost* 2004; **91**: 1257–8.
9 Bongers TN, De Maat MP, Dippel DW, Uitterlinden AG, Leebeek FW. Absence of Pro475Ser polymorphism in ADAMTS-13 in Caucasians. *J Thromb Haemost* 2005; **3**: 805.
10 Kokame K, Nobe Y, Kokubo Y, Okayama A, Miyata T. FRETS-VWF73, a first fluorogenic substrate for ADAMTS13 assay. *Br J Haematol* 2005; **129**: 93–100.
11 Groot E, Hulstein JJ, Rison CN, de Groot PG, Fijnheer R. FRETS-VWF73: a rapid and predictive tool for thrombotic thrombocytopenic purpura. *J Thromb Haemost* 2006; **4**: 698–9.
12 Kremer Hovinga JA, Mottini M, Lämmle B. Measurement of ADAMTS-13 activity in plasma by the FRETS-VWF73 assay: comparison with other assay methods. *J Thromb Haemost* 2006; **4**: 1146–8.
13 Mahdian R, Rayes J, Girma JP, Houllier A, Obert B, Meyer D, Veyradier A. Comparison of FRETS-VWF73 to full-length VWF as a substrate for ADAMTS13 activity measurement in human plasma samples. *Thromb Haemost* 2006; **95**: 1049–51.
14 Miyata T, Kokame K, Banno F, Shin Y, Akiyama M. ADAMTS13 assays and ADAMTS13-deficient mice. *Curr Opin Hematol* 2007; **14**: 277–83.
15 Furlan M, Robles R, Solenthaler M, Wassmer M, Sandoz P, Lämmle B. Deficient activity of von Willebrand factor-cleaving protease in chronic relapsing thrombotic thrombocytopenic purpura. *Blood* 1997; **89**: 3097–103.
16 Matsumoto M, Yagi H, Ishizashi H, Wada H, Fujimura Y. The Japanese experience with thrombotic thrombocytopenic purpura-hemolytic uremic syndrome. *Semin Hematol* 2004; **41**: 68–74.

Multiple anti-atherosclerotic treatments impair aspirin compliance: effects on aspirin resistance

P. PIGNATELLI,* S. DI SANTO,* F. BARILLÀ,† C. GAUDIO† and F. VIOLI*
**IV Clinical Division, Department of Experimental Medicine; and †Department of the Heart and Great Vessels Attilio Reale, University 'La Sapienza', Rome, Italy*

To cite this article: Pignatelli P, Di Santo S, Barillà F, Gaudio C, Violi F. Multiple anti-atherosclerotic treatments impair aspirin compliance: effects on aspirin resistance. *J Thromb Haemost* 2008; **6**: 1832–4.

The antithrombotic effect of aspirin has been well documented in patients with acute and chronic coronary syndromes [1]. Recently, the term 'aspirin resistance' was coined to describe aspirin-treated patients who respond to platelet agonists in aggregometric tests (residual platelet reactivity), or who have recurrence of cardiovascular events (CVEs) [2]. In a recent meta-analysis, a mean prevalence of aspirin resistance of about 25% was reported in CVE patients [3]. However, the definition of aspirin resistance has been based essentially on laboratory tests, which only in part depend on the platelet formation of thromboxane (Tx) A_2.

In clinical studies in which arachidonic acid (AA)-induced platelet aggregation (PA) and/or serum TxB_2 were investigated, the rate of aspirin resistance ranged from 2% to 43% [4,5]. The reason for this large variability remains unclear. An important issue, which so far has not been fully explored, is whether poor aspirin compliance might play a major role in aspirin resistance [6]. Two studies that specifically addressed this issue demonstrated that compliance had a major role [7,8]. Thus, in patients who were resistant to aspirin, inhibition of PA was fully restored when analysis of patients' adherence to aspirin treatment was performed. However, in these studies only AA-induced PA was used to explore aspirin resistance. No direct measure of platelet TxA_2, considered a prerequisite to analyze the rate of COX1 and eventually aspirin resistance, was provided [9]. Here, we undertook a prospective study to further evaluate the role of compliance on aspirin resistance intended as residual platelet reactivity.

An exploratory study was performed in 20 aspirin-treated patients at risk or with stable cardiovascular disease. AA-induced PA and serum TxB_2 (a stable metabolite of TxA_2) were measured after seven days of controlled aspirin (100 mg) intake. Aspirin was given by a doctor or a nurse to each patient.

AA (1 mM)-induced PA and serum TxB_2 were determined as previously described [10]. Briefly, PA was expressed as light transmission difference (% LT) between platelet-rich plasma

Correspondence: Francesco Violi, IV Clinical Division, Policlinico Umberto I, Università 'La Sapienza', Rome, Italy.
Tel.: +39 6 4461933; fax: +39 6 49970893.
E-mail: francesco.violi@uniroma1.it

DOI: 10.1111/j.1538-7836.2008.03122.x

Received 14 July 2008, accepted 24 July 2008

Novel System Evaluating In Vivo Pathogenicity of Desmoglein 3-Reactive T Cell Clones Using Murine Pemphigus Vulgaris[1]

Hayato Takahashi,* Masayuki Amagai,* Takeji Nishikawa,* Yoshiko Fujii,* Yutaka Kawakami,† and Masataka Kuwana[2‡]

Autoreactive T cells are thought to be involved in the pathogenesis of autoimmune diseases, but evidence for their direct pathogenicity is almost lacking. Herein we established a unique system for evaluating the in vivo pathogenicity of desmoglein 3 (Dsg3)-reactive T cells at a clonal level in a mouse model for pemphigus vulgaris (PV), an autoimmune blistering disease induced by anti-Dsg3 autoantibodies. Dsg3-reactive $CD4^+$ T cell lines generated in vitro were adoptively transferred into Rag-$2^{-/-}$ mice with primed B cells derived from Dsg3-immunized Dsg$3^{-/-}$ mice. Seven of 20 T cell lines induced IgG anti-Dsg3 Ab production and acantholytic blister, a typical disease phenotype, in recipient mice. Comparison of the characteristics between pathogenic and nonpathogenic Dsg3-reactive T cell lines led to the identification of IL-4 and IL-10 as potential factors associated with pathogenicity. Further in vitro analysis showed that IL-4, but not IL-10, promoted IgG anti-Dsg3 Ab production by primed B cells. Additionally, adenoviral expression of soluble IL-4Rα in vivo suppressed IgG anti-Dsg3 Ab production and the PV phenotype, indicating a pathogenic role of IL-4. This strategy is useful for evaluating the effector function of autoreactive T cells involved in the pathogenesis of various autoimmune diseases. *The Journal of Immunology,* **2008, 181: 1526–1535.**

Autoreactive T cells are thought to play a central role in the pathogenesis of various autoimmune diseases (1). A number of studies using patient samples and animal models have identified and characterized the autoreactive T cells that potentially exert the pathogenic effector function. Recent reports using autoreactive T cell clones generated from patient samples indicate that a subset of autoreactive T cells has a pathogenic effector function in vitro (2). However, it has been difficult to evaluate whether the individual autoreactive T cells analyzed in vitro are actually involved in the autoimmune pathogenic process of patients in vivo. Autoreactive T cell clones have been shown to induce tissue damage in a mouse model for multiple sclerosis and insulin-dependent diabetes mellitus (3, 4), but the in vivo helper activity of autoreactive T cells has never been analyzed at a clonal level in mouse models for autoantibody-mediated autoimmune diseases.

Pemphigus vulgaris (PV)[3] is a life-threatening blistering disease involving IgG autoantibodies directed against desmoglein 3 (Dsg3). Dsg3 is a cadherin-type glycoprotein expressed on stratified squamous epithelium, including the skin and oral mucosa, and plays a critical role in cell-cell adhesion (5). Anti-Dsg3 autoantibodies bind to keratinocyte cell surfaces and induce cell detachment, resulting in blisters and erosions in the skin and mucous membranes as well as characteristic histological findings, such as suprabasilar acantholysis (6, 7). Dsg3-reactive $CD4^+$ T cells have been detected and characterized in PV patients and healthy individuals, but it remains unclear whether these autoreactive T cells can induce the PV phenotype in vivo. In this study, we developed a novel experimental system that evaluates the in vivo pathogenicity of individual Dsg3-reactive T cell clones. In this system, Dsg3-reactive T cell lines generated in vitro from Dsg$3^{-/-}$ mice were adoptively transferred into recipient immunodeficient Rag-$2^{-/-}$ mice (Dsg$3^{+/+}$) to examine whether T cell lines have the ability to induce the PV phenotype after adoptive transfer. Using this system, we identified IL-4 as a critical T cell-derived factor involved in the pathogenesis of PV.

Materials and Methods

Mice

Dsg$3^{-/-}$ mice with a mixed genetic background of 129/SV (H-2^b) and C57BL/6J (H-2^b) were obtained by mating male and female Dsg$3^{-/-}$ mice (The Jackson Laboratory) (8). C57BL/6 mice and C57BL/6 Rag-$2^{-/-}$ mice were purchased from the Central Institute for Experimental Animals (Tokyo, Japan). OT-II (OVA-specific) TCR transgenic mice (H-2^b) were originally generated by Barnden et al. (9), and Rag-$2^{-/-}$ OT-II transgenic mice (H-2^b) were kindly provided by Prof. S. Koyasu (Keio University). The Keio University Ethics Committee for Animal Experiments approved all experiments in this study.

Antigens

A baculoprotein rDsg3EHis, which includes the extracellular domain of mouse Dsg3 (amino acid residues 1–565), an E-tag, and a His-tag, was produced as described previously (10) with some modifications. In brief, the purification was improved by serial procedures using Talon affinity metal resin (Clontech Laboratories) followed by a HiTrap anti-E Tag column (GE Healthcare). Five mouse Dsg3 fragments (rDsg3-1–5) expressed in *Escherichia coli* were prepared as soluble maltose-binding protein (MalBP)-Dsg3 fusion proteins as described (11). The Dsg3 fragments encompassing together the entire 565-aa sequence of the extracellular domain of mouse Dsg3 included rDsg3-1 (aa 1–119), rDsg3-2 (aa 99–230),

*Department of Dermatology, †Institute for Advanced Medical Research, and ‡Division of Rheumatology, Department of Internal Medicine, Keio University School of Medicine, Tokyo, Japan

Received for publication January 30, 2008. Accepted for publication May 13, 2008.

The costs of publication of this article were defrayed in part by the payment of page charges. This article must therefore be hereby marked *advertisement* in accordance with 18 U.S.C. Section 1734 solely to indicate this fact.

[1] This work was supported by Grants-in-Aid for Scientific Research from the Ministry of Education, Culture, Sports, Science and Technology of Japan, the Health and Labour Sciences Research Grants for Research on Measures for Intractable Diseases from Ministry of Health, Labor and Welfare of Japan, and Keio Gakuji Academic Development Funds.

[2] Address correspondence and reprint requests to Dr. Masataka Kuwana, Division of Rheumatology, Department of Internal Medicine, Keio University School of Medicine, 35 Shinanomachi, Shinjuku-ku, Tokyo 160-8582, Japan. E-mail address: kuwanam@sc.itc.keio.ac.jp

[3] Abbreviations used in this paper: Dsg3, desmoglein 3; PV, pemphigus vulgaris; MalBP, maltose-binding protein.

Table 1. *Primer sequences, optical annealing temperatures, and amplified sizes of genes analyzed in PCR*

Genes	Primers (5′ to 3′)	Annealing Temp. (°C)	Sizes (bp)
IL-2			
Sense	TGATGGACCTACAGGAGCTCCTGAG	60	168
Antisense	GAGTCAAATCCAGAACATGCCGCAG		
IL-4			
Sense	CGAAGAACACCACAGAGAGTGAGCT	60	181
Antisense	GACTCATTCATGGTGCAGCTTATCG		
IL-6			
Sense	CTGGTGACAACCACGGCCTCCCCT	60	601
Antisense	ATGCTTAGGCATAACGCACTAGGT		
IL-10			
Sense	TGAAGCTTCTATTCTAAGGCTGGCC	60	178
Antisense	CTGAGCTGCTGCAGGAATGATCATC		
IL-17			
Sense	GGTCAACCTCAAAGTCTTTAACTC	51	396
Antisense	AAATACAAGTAAGTTTGCTGAGAAACG		
IFN-γ			
Sense	GCTACACACTGCATCTTGGCTTTGC	60	939
Antisense	CCTGTTACTACCTGACACATTCGAG		
TGF-β			
Sense	GCTCACTGCTCTTGTGACAGCAAAG	60	362
Antisense	CAAGGACCTTGCTGTACTGTGTGTC		
CCR4			
Sense	GACTGTCCTCAGGATCACTTTCAGA	60	255
Antisense	CCCAACAAGAAGACCAAGGAGTAG		
CCR7			
Sense	AACCAAAAGCACAGCCTTCCTGT	60	299
Antisense	TGTACGTCAGTATCACCAGCCC		
CXCR3			
Sense	AAAGGCAGAGAAGCAGGCA	60	1275
Antisense	TTCAGGCTGAAATCCTGTGG		
CXCR5			
Sense	ATGGATGACCTGTACAAGGAACTG	60	282
Antisense	TGCAAAAGGCAGGATGAAGAC		
CRTH2			
Sense	GACAACTGCTCTCTAGGAGGAACT	60	1263
Antisense	ACCACAAACAGGATGAGTCCGT		
β-actin			
Sense	TGGAATCCTGTGGCATCCATGAAAC	60	227
Antisense	TAAAACGCAGCTCAGTAACAGTCCG		

rDsg3-3 (aa 210–345), rDsg3-4 (aa 325–455), and rDsg3-5 (aa 428–565). These recombinant proteins were dialyzed against PBS containing 0.5 mM $CaCl_2$, filter-sterilized, and stored at −80°C until use. The expression of recombinant Dsg3 fragments was evaluated by SDS-PAGE followed by Coomassie blue staining or immunoblotting probed with an anti-mouse Dsg3 mAb (AK7 or AK18) (7).

Recombinant adenovirus harboring Dsg3 and soluble cytokine receptors

Adenoviral vectors harboring the entire extracellular domain and transmembrane region of mouse Dsg3 (rDsg3ΔIC; aa 1–590) or the extracellular domain of cytokine receptors (IL-4Rα, IL-10Rα, and IFN-γR1) were constructed using the AdEasy adenoviral vector system (Stratagene) according to the manufacturer's instructions. rDsg3ΔIC was adenovirally expressed in COS cells, which were subjected to sonication in PBS containing 0.5 mM $CaCl_2$ and 0.01% Triton X-100. The cellular lysates were filter-sterilized and used in T cell cultures as a source of Dsg3. The expression of Dsg3 was evaluated by SDS-PAGE followed by immunoblotting with anti-mouse Dsg3 mAb and rabbit anti-actin polyclonal Ab (Sigma-Aldrich). For soluble cytokine receptors, the cDNA for the entire extracellular domain of each cytokine receptor was cloned from a spleen cDNA library and used to construct recombinant adenoviruses. Each recombinant adenovirus harboring a soluble cytokine receptor was concentrated by $CsCl_2$ density gradient centrifugation, dialyzed against PBS, and stocked at −80°C until use. The in vivo expression of soluble cytokine receptors was confirmed by immunoblotting plasma obtained from adenovirus-infected mice with goat anti-IL-4Rα, anti-IL-10Rα, or anti-IFN-γR1 polyclonal Abs (R&D Systems).

Ag-specific T cell lines

Footpads of $Dsg3^{-/-}$ mice were immunized with 5 μg of rDsg3EHis emulsified with CFA (Sigma-Aldrich). After 7 days, a single-cell suspension (3×10^6/well) was prepared from the popliteal lymph nodes and cultured in 24-well plates with a mixture of rDsg3-1–5 (5 μg/ml each) in complete medium (RPMI 1640, 2 mM L-glutamine, 1 mM pyruvate, 50 U/ml penicillin, and 50 μg/ml streptomycin) supplemented with 1% C57BL/6 mouse serum. The cells were stimulated twice with the mixture of rDsg3-1–5 in the presence of 10^6 autologous 40 Gy-irradiated splenocytes in complete medium containing 10% FBS (Cambrex). T-STIM without Con A (BD Biosciences) was added to a final concentration of 1% twice a week as a source of growth factors. T cell blasts were subsequently subjected to limiting dilution using round-bottom 96-well plates in the presence of irradiated autologous splenocytes (2×10^4/well), antigenic Dsg3 fragments, and 1% T-STIM without Con A.

T cell proliferation assay

Dsg3-specific T cell proliferation was measured by [^{3}H]thymidine uptake as described (11). In some experiments, bone marrow-derived dendritic cells, which were prepared by culturing C57BL/6 bone marrow cells with 10 ng/ml GM-CSF (PeproTech) for 7 days, were used as APCs. Before the coculture with T cells, the bone marrow-derived dendritic cells were pulsed with pAd-rDsg3ΔIC or mock vector-transduced COS cell lysates (100 μg/ml) and maturated with 10 μg/ml LPS (Sigma-Aldrich) for 24 h. MHC class II restriction was determined by evaluating the inhibitory effect on Ag-induced T cell proliferation of 4 μg/ml rat anti-I-A^b mAb (clone M5/114; BD Biosciences). An isotype-matched rat mAb to an irrelevant Ag (BD Biosciences) was used as a control.

Passive transfer

To evaluate the pathogenicity of Dsg3-reactive T cell lines, Dsg3-reactive T cell lines (10^6) and splenic $Dsg3^{-/-}$ B cells (5×10^6) were transferred into Rag-$2^{-/-}$ mice via the tail vein. In vivo-primed $Dsg3^{-/-}$ B cells were prepared by depleting $CD4^+$ and $CD8^+$ cells from the splenocytes of rDsg3EHis-immunized $Dsg3^{-/-}$ mice (10), followed by the positive selection of $B220^+$

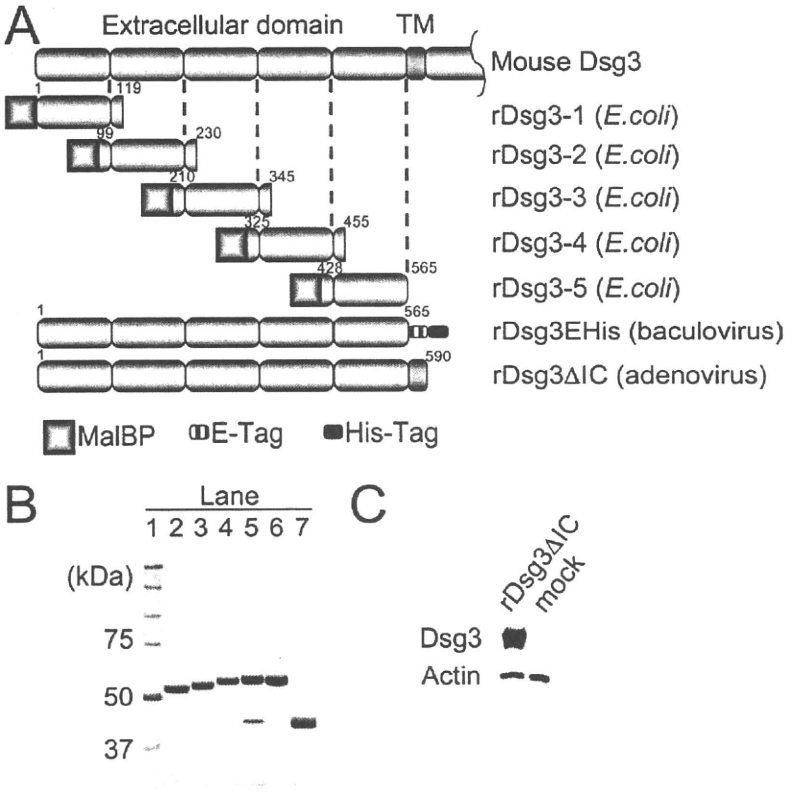

FIGURE 1. Recombinant mouse Dsg3 proteins. *A*, Schematic illustration of the mouse Dsg3 and recombinant Dsg3 proteins used in this study. rDsg3-1–5 are bacterial recombinant Dsg3 fragments fused to MalBP. rDsg3EHis is a baculovirally produced Dsg3 extracellular domain with an E-tag and His-tag at the carboxyl terminus. rDsg3ΔIC is adenovirally produced Dsg3 lacking the intracellular domain. The numbers indicate the positions of amino acid residues in Dsg3. TM, transmembrane domain. *B*, rDsg3-1–5 and MalBP visualized by Coomassie blue staining. *Lane 1*, molecular mass markers; *lanes 2–6*, rDsg3-1–5; *lane 7*, MalBP (*lane 7* is a different part of the same gel). *C*, Immunoblots of lysates from cells infected with the rDsg3ΔIC-harboring adenovirus vector or mock virus. Fractionated proteins were probed with anti-mouse Dsg3 or anti-actin Ab.

cells using the MACS cell separation system (Miltenyi Biotec). A portion of the separated $CD4^+$ and $CD8^+$ cells was used as unfractionated $Dsg3^{-/-}$ T cells. In some experiments, recombinant adenovirus harboring sIL-4Rα, sIL-10Rα, or sIFN-γR1 (10^9 infections units) was directly injected into Rag-$2^{-/-}$ mice via tail vein 5 days before the passive transfer of pathogenic Dsg3-reactive T cell clones and $Dsg3^{-/-}$-primed B cells. It has been demonstrated that recombinant adenovirus injected from tail vein mainly infects hepatocytes, resulting in expression of recombinant protein (12).

RT-PCR

T cell lines were stimulated with 25 ng/ml PMA (Sigma-Aldrich) and 1 μg/ml ionomycin (Sigma-Aldrich) for 3 days, and isolated using anti-CD4 mAb-coupled magnetic beads (Dynal Biotech). Total RNA was isolated from individual T cell lines using the RNeasy mini kit with RNase-free DNase (Qiagen). For the analysis of TCR Vβ gene usage, aliquots of the synthesized cDNA (5 ng of total RNA equivalent) were amplified using a

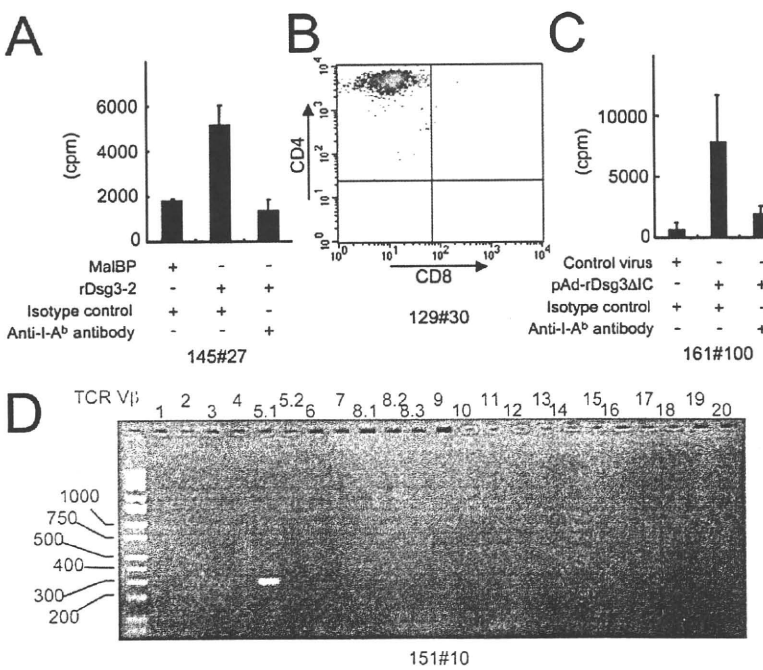

FIGURE 2. Characterization of representative Dsg3-reactive T cell lines. *A*, Dsg3-specific proliferative response of T cell line 145#27, which responded to rDsg3–2 in an I-A^b-specific manner. *B*, Surface expression of CD4 and CD8 by T cell clone 129#30 examined by flow cytometry. *C*, Proliferative responses of T cell line 161#100 to DC pulsed with cellular lysates infected with either rDsg3ΔIC or control adenovirus. *D*, Expression of a single functional TCR Vβ gene Vβ5.1 in Dsg3-reactive T cell clone 151#10, analyzed by family PCR using a series of TCR Vβ gene-specific primers.

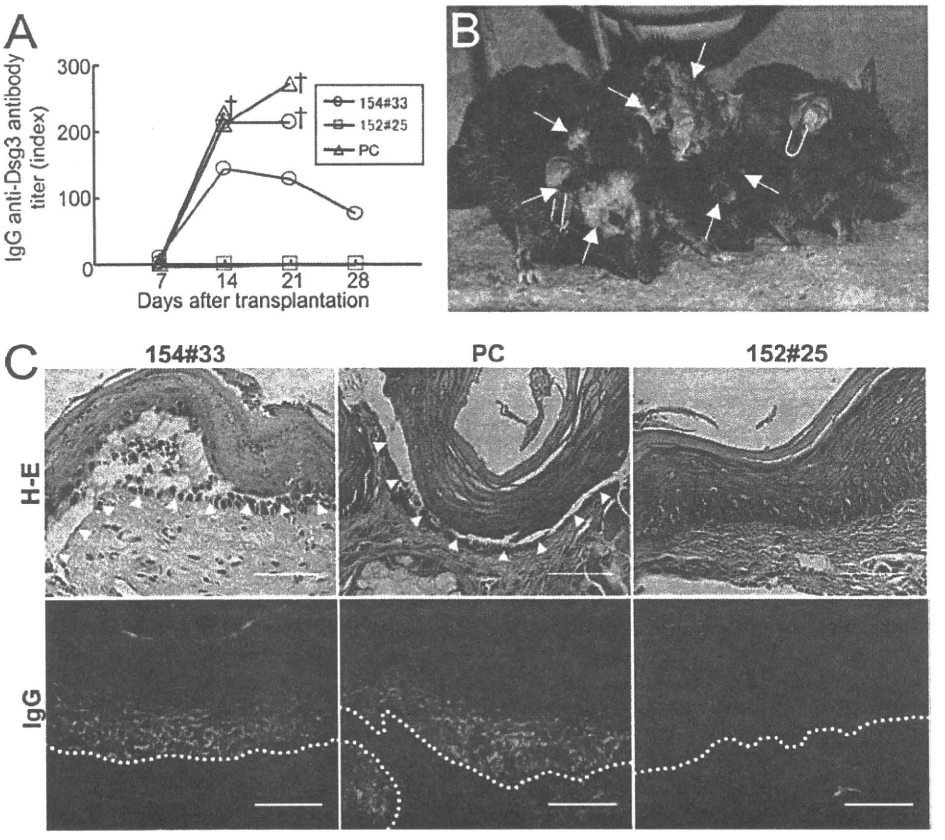

FIGURE 3. Evaluation of the in vivo pathogenicity of Dsg3-reactive T cell clones. *A*, Serial changes in the levels of IgG anti-Dsg3 Abs in mice that had been treated with the adoptive transfer of the Dsg3-reactive T cell clone 152#25 (□) or 154#33 (○). Mice were treated with $Dsg3^{-/-}$ unfractionated T cells as a positive control (PC, △). *B*, Skin phenotype of mice treated with 154#33 (*left*), $Dsg3^{-/-}$ T cells (*center*), or 152#25 (*right*) on day 22. Erosions and hair loss (arrows) were apparent in the periorbital area, nose, head, ears, and shoulders of mice treated with 154#33 or $Dsg3^{-/-}$ T cells. *C*, Histology (*upper panels*) and IgG deposition (*lower panels*) in the palate from recipient mice. Acantholytic blister (arrowheads) and IgG deposition on keratinocyte cell surfaces were observed in the 154#33-treated mouse, as observed in the $Dsg3^{-/-}$ T cell-treated mouse. Dotted lines indicate the basement membrane. Bars: 50 μm.

panel of TCR Vβ region-specific primers in combination with a Cβ region primer for 37 cycles. Primers for Vβ1–20 and Cβ were designed based on previous reports (13–15). The expression of cytokines and chemokine receptors was also examined by PCR using the specific primers listed in Table I for 38 and 40 cycles, respectively.

Flow cytometry

Surface markers of the Dsg3-reactive T cell lines were analyzed using FITC-conjugated anti-mouse CD4 mAb (clone GK1.5), FITC-conjugated anti-mouse CD8 mAb (clone 53-6.7), PE-conjugated anti-mouse TCRβ

Table II. *Characteristics of Dsg3-reactive T cell lines according to their in vivo pathogenicity*

Line Name	Antigenic Fragments	Functional TCR Vβ Gene Usage (Vβ)	Cytokine Expression							Chemokine Receptor Expression					In Vivo Production of Anti-Dsg3 Antibody
			IL-2	IL-4	IL-6	IL-10	IL-17	IFN-γ	TGF-β	CCR7	CCR4	CXCR5	CRTH2	CXCR3	
T cell lines with in vivo pathogenicity[a]															
140#27[b]	rDsg3-3	6	+	+	−	+	+	+	+	−	+	−	−	+	+
147#27[b]	rDsg3-3	8.2	+	+	+	+	−	+	+	+	+	+	−	+	+
147#48[b]	rDsg3-3	8.2	+	+	+	+	−	+	+	+	+	−	−	+	+
153#5	rDsg3-1	5, 7, 8.1	+	+	−	+	−	+	+	+	+	−	−	+	+
154#33[b]	rDsg3-1	8.2	+	+	+	+	+	+	+	+	+	+	−	+	+
161#100	rDsg3-1	6, 11	+	+	−	+	−	+	+	+	+	+	−	+	+
164#2[b]	rDsg3-3	6	+	+	−	+	−	+	+	+	+	−	−	+	+
T cell lines without in vivo pathogenicity[a]															
129#30[b]	rDsg3-3	8.3	+	−	−	−	−	+	+	+	+	−	−	+	−
141#70[b]	rDsg3-1	6	+	−	−	−	−	+	+	+	−	+	−	+	−
145#27	rDsg3−2, 4	6, 14	+	−	−	−	−	+	−	−	−	−	−	−	−
145#28	rDsg3-1	8.2, 11	+	+	+	+	−	+	+	−	−	−	−	+	−
146#13	rDsg3-2	1, 4	+	+	+	+	+	+	+	+	+	+	−	+	−
146#25	rDsg3-4	8.1, 15	+	−	−	+	−	+	−	−	−	+	−	−	−
151#10[b]	rDsg3-1	5.1	−	−	−	−	−	+	+	+	−	+	−	+	−
152#25[b]	rDsg3-1	1	−	+	−	−	−	+	+	+	+	−	−	+	−
159#11	rDsg3-1	3, 4	+	−	−	−	−	+	+	+	+	+	−	+	−
161#28[b]	rDsg3-2	6	+	+	−	+	+	+	+	+	+	+	−	+	−
161#29[b]	rDsg3-2	4	−	+	+	+	+	+	+	+	+	+	−	+	−
162#24[b]	rDsg3-1	8.1	+	−	−	−	+	+	+	+	+	+	+	+	−
162#92[b]	rDsg3-2	8.2	+	+	+	+	−	+	+	+	+	+	−	+	−

[a] Identification of in vivo pathogenicity requres anti-Dsg3 Ab production, IgG deposition on the epithelial cell surfaces of the palate, and acantholysis.
[b] Clonality was confirmed by TCR β-chain analysis.

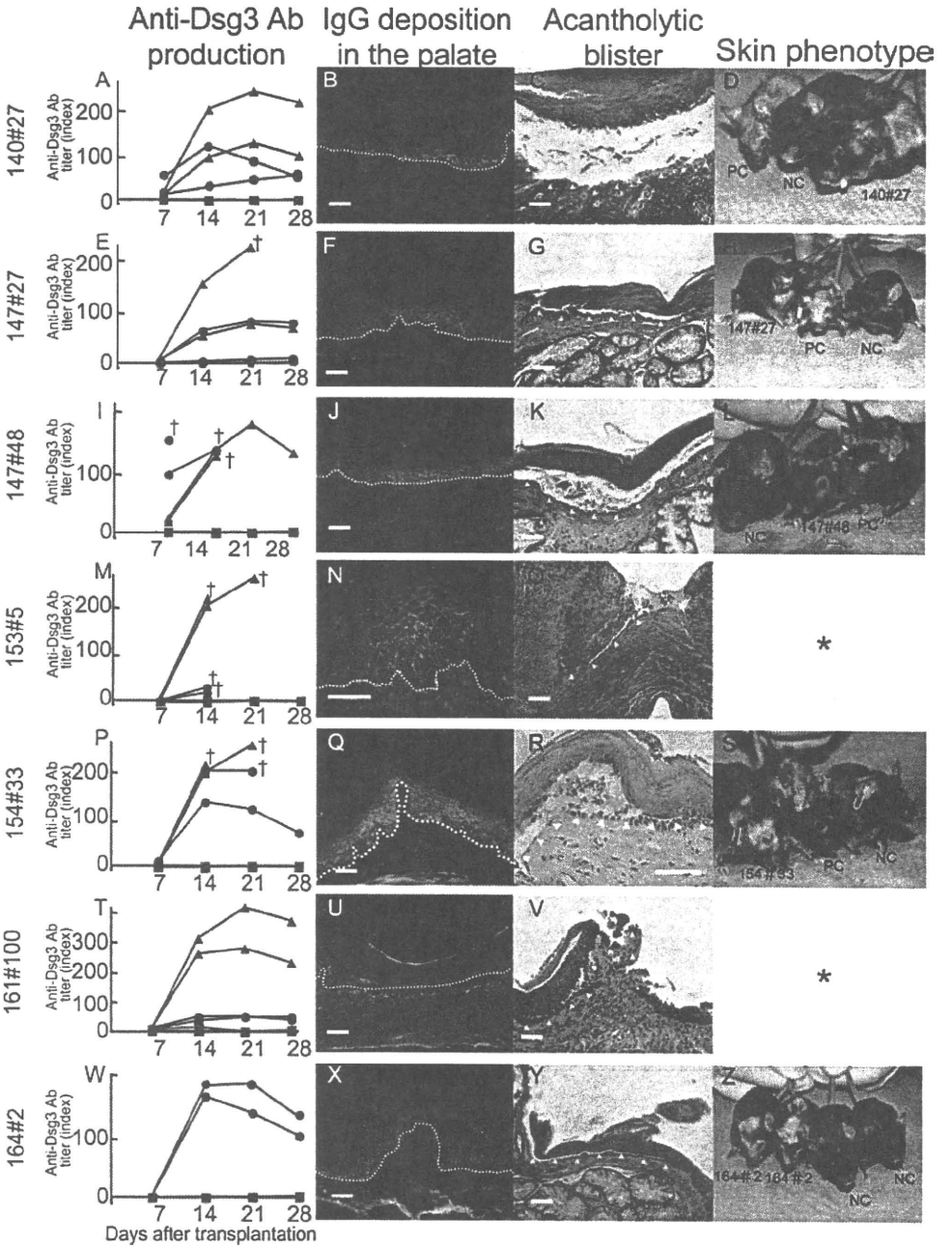

FIGURE 4. Anti-Dsg3 Ab production, IgG deposition in the palate, acantholytic blisters, and skin phenotype induced by individual Dsg3-reactive T cell lines with in vivo pathogenicity. 140#27, 147#27, 147#48, 154#33, and 164#2 were confirmed to be clones. *A*, *E*, *I*, *M*, *P*, *T*, and *W*, In the anti-Dsg3 Ab ELISA, the blue lines indicate mice with the transplanted T cell lines of interest, black lines indicate the positive control mice with transplanted $Dsg3^{-/-}$ T cells, and red lines indicate the negative control mice with transplanted B cells alone (*A* and *E*) or B cells in combination with a nonpathogenic clone 161#28 (*I*), 152#25 (*M*, *P*, and *T*), or 161#29 (*W*). Crosses indicate death. *B*, *F*, *J*, *N*, *Q*, *U*, and *X*, IgG deposition (green) in the palate was detected by immunostaining with an AlexaFluor 488-conjugated anti-mouse IgG Ab. Dotted lines indicate basement membrane. *C*, *G*, *K*, *O*, *R*, *V*, and *Y*, Acantholytic blisters (arrowheads) in the palate were evaluated by H&E staining. *D*, *H*, *L*, *S*, and *Z*, PC denotes the positive control mouse, and NC denotes the negative control mouse. Bars: 50 μm. Asterisks indicate that images are unavailable.

mAb (clone H57-597), and Cy-Chrome-conjugated anti-mouse CD4 mAb (clone H129.19), all of which were purchased from BD Biosciences. In some experiments, T cell lines labeled with 1 μM CFSE (Molecular Probes) were analyzed by flow cytometry after gating on the $CD4^+TCR\beta^+$ population of the lymphocyte fraction.

Anti-Dsg3 Ab

IgG anti-Dsg3 Abs in plasma samples or culture supernatants were quantitatively measured using an ELISA as described previously (10). To examine the capacity of B cells to produce anti-Dsg3 Abs in vitro, MACS-sorted $Dsg3^{-/-}$ B cells were cultured with 500 ng/ml soluble CD40L (R&D Systems) in the presence of various concentrations of IL-4, IL-10, or IFN-γ (R&D Systems) for 7 days.

Histopathology

Formalin-fixed palate tissue was stained with H&E and observed with an inverted microscope TE2000-U (Nikon).

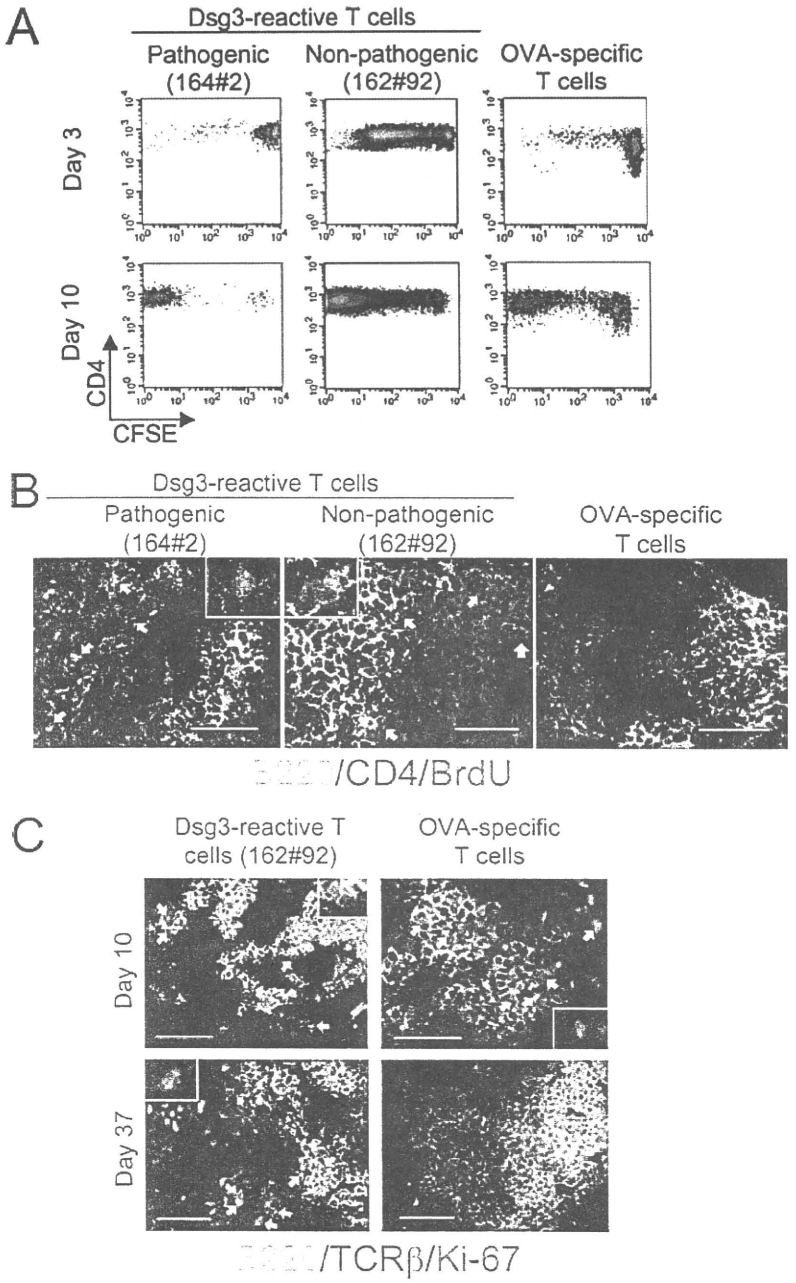

FIGURE 5. In vivo proliferative capacity of Dsg3-reactive T cell clones. *A*, Flow cytometric analysis of CFSE dilution in splenic $CD4^+TCR\beta^+$ T cells. After Dsg3-reactive T cell clone 164#2 (pathogenic), clone 162#92 (nonpathogenic), or OVA-specific T cells were labeled with CFSE in vitro, the T cells were transferred with $Dsg3^{-/-}$ B cells isolated from a Dsg3-immunized $Dsg3^{-/-}$ mouse into $Rag2^{-/-}$ mice. T cells were analyzed for CFSE dilution by flow cytometry after gating on the $CD4^+TCR\beta^+$ population of the splenocytes 3 and 10 days after transfer. *B*, Immunostaining for B220 (green), CD4 (blue), and BrdU (red) in the spleen from recipient mice 37 days after the transfer of Dsg3-reactive T cell clone 164#2 (pathogenic), clone 162#92 (nonpathogenic), or OVA-specific T cells. BrdU-bearing $CD4^+$ T cells (arrows) were detected in the region close to the B cell area in mice with transplanted Dsg3-reactive T cell lines. *C*, Immunostaining for B220 (green), TCRβ (blue), and Ki-67 (red) in the spleen from recipient mice on days 10 and 37 after the transfer of Dsg3-reactive T cell clone 162#92 or OVA-specific T cells. On day 37, Ki-67-positive T cells (arrows) were detected in mice with transplanted Dsg3-reactive T cell lines, but not in mice with transplanted OVA-specific T cells. Bars: 50 μm. Insets denote high-power views of T cells positive for BrdU or Ki-67.

Immunohistochemistry

For direct immunofluorescent staining, 10-μm cryosections of the palate were directly stained with AlexaFluor 488-conjugated anti-mouse IgG Abs (Molecular Probes) and observed using a fluorescence microscope (Nikon) to detect IgG deposits. For indirect staining, 6-μm cryosections of the spleen were fixed with acetone and subsequently stained with the appropriate combination of the following Abs: FITC-conjugated anti-mouse CD19 (clone 1D3), PE-conjugated anti-mouse TCRβ (clone H57-597), AlexaFluor 488-conjugated anti-mouse B220 (clone RA3-6B2), biotinylated anti-mouse CD4 (clone RM4-5, BD Biosciences), and anti-Ki-67 mAb (clone TEC-3; DakoCytomation). Secondary Abs included AlexaFluor 488-conjugated anti-mouse IgG, AlexaFluor 660-conjugated anti-rat IgG, and AlexaFluor 488-conjugated anti-FITC Abs, and AlexaFluor 568-conjugated streptavidin (Molecular Probes). BrdU staining was performed using AlexaFluor 660-conjugated anti-BrdU mAb (clone PRB-1, Molecular Probes), as previously described (16). Sections were observed under a confocal laser fluorescence microscope FV1000 (Olympus).

Statistical analysis

All continuous data are shown as the means ± SD. Two-tailed repeated-measures ANOVA, Fisher's exact probability test, or the Mann-Whitney *U* test was used as appropriate.

Results

Preparation of recombinant Dsg3 proteins

We prepared recombinant mouse Dsg3 fragments using three different expression systems (Fig. 1*A*). rDsg3EHis (10), a baculoprotein containing the entire extracellular domain of Dsg3, was used to immunize $Dsg3^{-/-}$ mice. rDsg3-1–5, a series of recombinant MalBP-Dsg3 fusion proteins produced in *E. coli*, were used to expand Dsg3-reactive T cells and to evaluate antigenic regions in vitro. The purity of each recombinant protein was >95% (Fig. 1*B*).

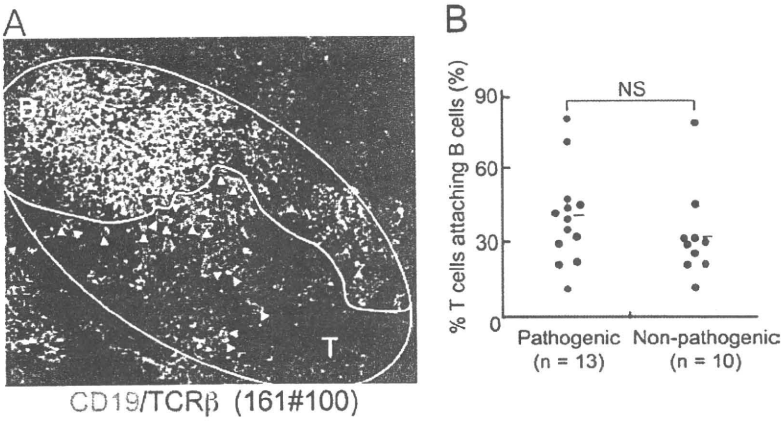

FIGURE 6. In vivo homing of transferred Dsg3-reactive T cell lines in the spleen. *A*, A representative image of CD19 (green) and TCRβ (red) in the spleen of mice with transplanted Dsg3-reactive T cell line 161#100. Based on the distribution of CD19 and TCRβ staining, the Dsg3-reactive T cells were classified into T cells within the B cell area (pink arrowheads) and those residing outside the B cell area (yellow arrowheads). The T cell area (T) and B cell area (B) are indicated with white outlines. *B*, The proportion of T cells within the B cell area of the total T cells in the spleen from mice with transplanted Dsg3-reactive T cell lines, according to the presence or absence of in vivo pathogenicity. A total of 165 lymphoid follicle-like structures were analyzed. Values were averaged in 23 individual mice and compared between the pathogenic (147#48, 153#5, 161#100, and 164#2) and nonpathogenic T cell lines (146#13, 152#25, 159#11, 161#28, and 162#24). Statistical analysis was performed by the Mann-Whitney *U* test. Horizontal bars indicate the mean.

Lysates from COS cells infected with pAd-rDsg3ΔIC, an adenovirus vector harboring Dsg3 cDNA lacking the sequence for the intracellular domain, were used to evaluate T cell reactivity to native Dsg3 produced in mammalian cells (Fig. 1*C*). Serial use of more than one Dsg3 preparation for T cell stimulation is useful to eliminate expansion of T cells responsive to contaminant proteins unique to individual Ag preparations.

Establishment of Dsg3-reactive T cell lines

To establish Dsg3-reactive T cell lines, the footpads of Dsg3$^{-/-}$ mice were immunized with rDsg3EHis emulsified with CFA. Single-cell suspensions of lymphocytes were prepared from the popliteal lymph nodes and were subsequently stimulated twice with a mixture of rDsg3-1–5 in vitro. The expanded cells that showed a specific proliferative response to at least one of the Dsg3 fragments were subjected to limiting dilution. From this selection, we obtained 59 T cell lines that were specifically reactive with one of rDsg3-1–4. All of these T cell lines were restricted by MHC class II (Fig. 2*A*) and expressed the CD4 surface marker (Fig. 2*B*). To evaluate whether these T cell lines responded to peptides generated from native Dsg3 through Ag processing, randomly selected T cell lines were cultured with bone marrow-derived dendritic cells pulsed with pAd-rDsg3ΔIC-infected and control adenovirus-infected cell lysates. All the T cell lines examined showed a specific response to Dsg3-expressing cell lysates in a MHC class II-dependent manner (Fig. 2*C*). The in vitro-generated T cell lines were reactive to two different Dsg3 preparations, indicating that they were specific for Dsg3. Eighteen Dsg3-reactive T cell lines were confirmed to be clones based on their expression of a single functional TCR Vβ-chain, determined by family PCR combined with a direct nucleotide sequencing (Fig. 2*D*).

In vivo pathogenicity of Dsg3-reactive T cell lines

Twenty Dsg3-reactive T cell lines, including 13 clones expressing single functional TCR Vβ-chain, were further evaluated for their in vivo pathogenicity. Since our previous study demonstrated that splenic T cells and B cells are required to induce experimental PV (17), the individual T cell lines were transferred into Rag-2$^{-/-}$ mice together with primed B cells isolated from the spleen of a rDsg3EHis-immunized Dsg3$^{-/-}$ mouse. In a representative experiment, clone 154#33 effectively promoted the production of IgG anti-Dsg3 Abs in vivo (Fig. 3*A*) and subsequently induced a PV phenotype, consisting of skin erosions and hair loss (Fig. 3*B*). Mice into which clone 154#33 was transferred showed acantholytic blisters and in vivo IgG deposition on keratinocyte cell surfaces (Fig. 3*C*). These PV features were also observed in positive control mice, into which unfractionated Dsg3$^{-/-}$ T cells had been transferred instead of Dsg3-reactive T cell lines. In contrast, transplantation of another clone, 152#25, failed to induce the IgG anti-Dsg3 Ab production or the PV phenotype, indicating that only a subset of the Dsg3-reactive T cell lines possessed in vivo pathogenic activity. The PV phenotype was not observed in control mice that received primed Dsg3$^{-/-}$ B cells alone or in combination with irrelevant OVA-specific T cells derived from Rag-2$^{-/-}$ OT-II transgenic mice (data not shown).

As summarized in Table II, 7 of the Dsg3-reactive T cell lines, including 5 clones, induced the PV phenotype in vivo, and thus were regarded as pathogenic lines; in contrast, 13 of the Dsg3-reactive T cell lines failed to induce the PV phenotype. A total of 86 mice were used for this analysis. Results regarding the PV phenotype induction were completely reproducible: none of the nonpathogenic T cell lines induced the PV phenotype despite several attempts. Detailed data on the anti-Dsg3 Ab production, histological findings, and skin phenotype in mice receiving transplants of six additional Dsg3-reactive T cell lines possessing in vivo pathogenicity are shown in Fig. 4. Interestingly, the in vivo production of IgG anti-Dsg3 Abs and the PV skin phenotype in mice receiving Dsg3-reactive T cell lines were completely concordant, suggesting a direct pathogenic role of the anti-Dsg3 Ab response in our PV model.

In vivo behavior of Dsg3-reactive T cells

To analyze the fate of the transferred autoreactive T cells, we examined whether the transplanted Dsg3-reactive T cells proliferated in vivo in the recipient Rag-2$^{-/-}$ mice, using several different systems. First, Dsg3-reactive or OVA-specific T cells were labeled with CFSE and transferred into Rag-2$^{-/-}$ mice in combination with primed Dsg3$^{-/-}$ B cells. On the 10th day after adoptive transfer, diluted CFSE was detected in the spleen of mice treated with pathogenic and nonpathogenic Dsg3-reactive T cell lines as well as

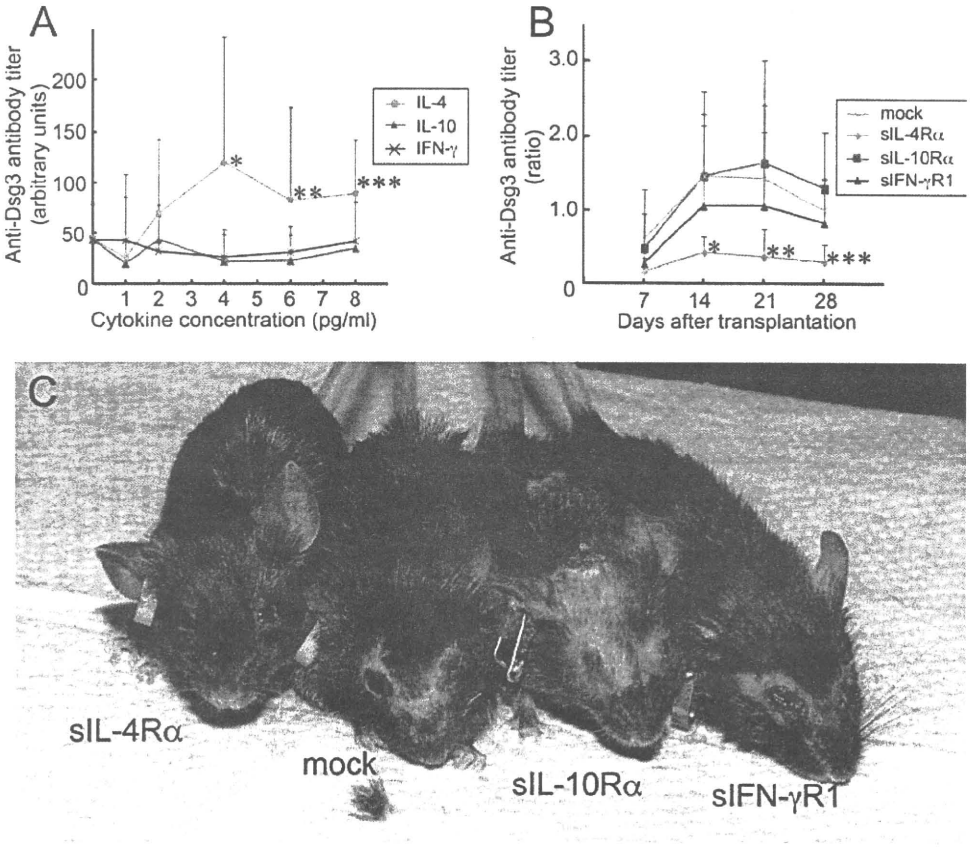

FIGURE 7. Role of T cell-derived cytokines in experimental PV. *A*, IgG anti-Dsg3 Ab titers in the culture supernatants of primed B cells. Splenic B cells from rDsg3EHis-immunized Dsg3$^{-/-}$ mice were cultured for 7 days with recombinant soluble CD40L in the presence of IL-4, IL-10, or IFN-γ at the concentrations indicated. Values shown are the means and SD of 16 individual experiments. Statistical analysis was performed by two-tail repeated measures ANOVA. *, $p = 0.0002$; **, $p = 0.008$; ***, $p = 0.01$. *B*, Effects of cytokine blockade on anti-Dsg3 Ab production in mice with transplanted Dsg3-reactive T cell clones. Serial IgG anti-Dsg3 Ab titers in plasma from mice expressing adenovirus-borne sIL-4Rα, sIL-10Rα, or sIFN-γR1 and subsequently undergoing adoptive transfer of pathogenic Dsg3-reactive T cell clone 147#48. Values are the mean and SD of six independent experiments, shown as a ratio to the Ab titer on day 28 in mock-treated mice. Statistical analysis was performed by two-tail repeated-measures ANOVA. *, $p = 0.03$; **, $p = 0.04$; ***, $p = 0.02$. *C*, Effects of cytokine blockade on the skin phenotype of mice 14 days after the adoptive transfer of pathogenic Dsg3-reactive T cell clone 147#48. Note the lack of erosion or hair loss in a mouse pretreated with adenovirus vector harboring sIL-4Rα.

those receiving irrelevant OVA-specific T cells (Fig. 5*A*), indicating that the transferred T cells were viable and expanded in vivo irrespective of their antigenic specificity or pathogenic activity. This early and nonspecific T cell proliferation was consistent with homeostatic proliferation (18, 19), which is a proliferative response of mature T cells in the lymphopenic environment to restore the lymphocyte pool size (20). Since it has been reported that the influence of homeostatic proliferation is negligible beyond 30 days of transfer (21), T cell proliferation was evaluated on day 37 by BrdU incorporation in the spleen of recipient mice. BrdU-bearing proliferating CD4$^+$ T cells were frequently detected in mice treated with Dsg3-reactive T cell lines irrespective of their pathogenicity, but not in mice treated with irrelevant OVA-specific T cells (Fig. 5*B*). The in vivo expansion of the Dsg3-reactive T cells was further evaluated by the expression of Ki-67, a marker for cell proliferation. In recipient mice, Dsg3-reactive and OVA-specific T cells expressed Ki-67 with similar frequencies on day 10, but Ki-67 expression was exclusively detected in the Dsg3-reactive T cells, irrespective of their pathogenicity, on day 37 (Fig. 5*C*). These findings together indicate that the transferred Dsg3-reactive T cells persistently proliferate in vivo, independent of their pathogenicity. Thus, the in vivo proliferative capacity did not account for the presence or absence of the in vivo pathogenicity of individual T cell lines.

Comparison of characteristics between Dsg3-reactive T cell lines with and without in vivo pathogenicity

Table II summarizes the antigenic Dsg3 fragments, functional TCR Vβ gene usage, and expression profiles of cytokines (IL-2, IL-4, IL-6, IL-10, IL-17, IFN-γ, and TGF-β) and chemokine receptors (CCR4, CCR7, CXCR3, CXCR5, and CRTH2) in the 20 Dsg3-reactive T cell lines evaluated for their pathogenicity, which included 13 clones. To identify T cell-derived factors associated with in vivo pathogenicity, the individual characteristics were compared between the 7 T cell lines with in vivo pathogenicity and the 13 lines without it. This analysis showed that all of the pathogenic T cell lines expressed IL-4 and IL-10, and the frequency of lines expressing IL-4 or IL-10 was significantly higher in the pathogenic than in the nonpathogenic group ($p = 0.045$ for both comparisons). There was no significant difference in the other characteristics between these two groups.

To examine the in vivo homing profiles of the transferred Dsg3-reactive T cell lines, spleen sections were stained with TCRβ for Dsg3-reactive T cells and with CD19 for B cells. Both the Dsg3-reactive T cell lines and the B cells had accumulated in the spleen and formed a lymphoid follicle-like structure. The Dsg3-reactive T cells were mainly detected in the T cell area, but some had infiltrated into the B cell area (Fig. 6*A*). There was no difference in the

number of T cells within the B cell area between mice treated with pathogenic T cell lines and those treated with nonpathogenic T cell lines (Fig. 6*B*), indicating that the presence or absence of pathogenicity in the Dsg3-reactive T cell lines was not due to a difference in the in vivo homing profiles.

A role of IL-4 in the pathogenesis of PV

We next assessed the roles of IL-4 and IL-10 released by Dsg3-reactive T cells in the mouse PV model, in vitro and in vivo. First, the IgG anti-Dsg3 Abs produced in vitro were measured in the culture supernatants of splenic B cells from rDsg3EHis-immunized Dsg3$^{-/-}$ mice stimulated with soluble recombinant CD40L in the presence of exogenous IL-4, IL-10, or IFN-γ. As shown in Fig. 7*A*, IL-4 significantly promoted the production of IgG anti-Dsg3 Abs from primed Dsg3$^{-/-}$ B cells, but neither IL-10 nor IFN-γ had such activity. Next, recombinant adenovirus harboring soluble cytokine receptors (IL-4Rα, IL-10Rα, or IFN-γR1) was administered to Rag-2$^{-/-}$ mice via the tail vein to neutralize IL-4, IL-10, or IFN-γ in vivo. Five days later, the pathogenic Dsg3-reactive T cell clone 147#48 and primed Dsg3$^{-/-}$ B cells were adoptively transferred into immunodeficient mice. The in vivo expression of soluble IL-4Rα significantly suppressed the IgG anti-Dsg3 Ab production (Fig. 7*B*) and the PV skin phenotype (Fig. 7*C*), but the expression of soluble IL-10Rα or soluble IFN-γR1 had no effect. Concordant results were obtained from six independent experiments using clone 147#48, and from four experiments using another pathogenic clone, 164#2.

Discussion

We successfully established a novel evaluation system for the in vivo pathogenicity of Ag-specific T cells at a clonal level, by performing the adoptive transfer of in vitro-generated Ag-specific T cell clones into immunodeficient Rag-2$^{-/-}$ mice in combination with in vivo-primed B cells. We confirmed that the transferred Dsg3-reactive T cells proliferated persistently and homed to the secondary lymphoid tissue in vivo, but only a subset of the T cell lines were able to induce the disease phenotype. Additionally, the capacity of Dsg3-reactive T cell lines to induce anti-Dsg3 Ab production was completely concordant with the PV phenotype expression, confirming previous reports showing that the anti-Dsg3 autoantibody has a direct role in inducing PV in human patients (6) and in a mouse model (7). More importantly, this study directly demonstrates that a single Ag-specific CD4$^+$ T cell is capable of inducing autoimmune disease phenotype through pathogenic autoantibody production. Finally, the classification of Dsg3-reactive T cell lines into pathogenic and nonpathogenic lines enabled us to identify T cell-derived IL-4 as a critical molecule driving PV in the mouse model. Our experimental system is applicable to other autoimmune diseases in which the autoimmune targets are identified, and it is useful not only for screening the in vivo pathogenicity of autoantigen-specific T cells, but also for identifying molecules and pathways critically involved in the pathogenic autoimmune process. The in vitro establishment of autoantigen-reactive T cell lines is the most time-consuming step in our procedure, but once specific T cell lines are available, their in vivo pathogenic activity and behavior can be readily evaluated.

Our in vivo finding that T cell-derived IL-4 plays a critical role in this mouse model of PV may also be relevant to human PV, because a previous report demonstrated the presence of Dsg3-reactive T cells capable of producing IL-4 in PV patients, but not in healthy controls (22). Since we showed that exogenous IL-4 directly stimulated B cells to produce anti-Dsg3 Abs in vitro, IL-4 produced by Dsg3-reactive T cells is likely to play an essential role in pathogenic anti-Dsg3 autoantibody production. Our results further indicate that IL-4 is essential but not enough to induce PV phenotype, because some of the nonpathogenic Dsg3-reactive T cell lines express IL-4. The pathogenic role of T cell-derived IL-4 has been previously investigated in mouse models for several autoantibody-mediated autoimmune diseases. For example, in experimental autoimmune myasthenia gravis, the disease phenotype is more severe and lasts longer in IL-4$^{-/-}$ mice, indicating a role for IL-4 in preventing the disease (23, 24). In this regard, it has been shown that acetylcholine receptor-reactive T cell clones generated from myasthenia gravis patients fail to secrete IL-4 (25), and that acetylcholine receptor-stimulated IL-4 secretion from PBMC is rarely detected in myasthenia gravis patients (26). Additionally, experimental Graves' disease can be induced in IFN-γ$^{-/-}$ mice, but not in IL-4$^{-/-}$ mice, indicating a requirement for IL-4 in disease induction (27), while IL-4 was shown to exert an inhibitory effect in another mouse model for Graves' disease (28). These inconsistent results suggest that the roles of IL-4 in the pathogenic processes of autoantibody-mediated autoimmune diseases are complex, but they may also reflect the limitation of studies using gene-deficient mice to evaluate the roles of cytokines in autoimmune pathogenesis. Congenital defects in systemic cytokine production are known to affect the physiologic development of the immune system. Moreover, IL-4 secreted by non-T cells could potentially regulate the autoimmune pathogenesis. Our system enables the in vivo effector function of autoreactive T cell clones to be evaluated without the influence of these factors.

It is unclear what determines the nature of Dsg3-reactive T cells in terms of pathogenicity. Our results clearly show that there were a wide variety of gene expression profiles among Dsg3-reacive T cell clones. This heterogeneity is probably generated in a hierarchy during T cell development, and Dsg3-reactive T cells with all of the quantitative and qualitative features required for the PV phenotype induction in our experimental system were regarded as pathogenic clones. Therefore, it is probable that nonpathogenic Dsg3-reactive T cell clones may be able to induce the PV phenotype when missing factors would be supplemented with an appropriate microenvironment. In this regard, it would be interesting to examine if transfer of a large number of the nonpathogenic T cell clone or transfer of the nonpathogenic T cell clone in the presence of exogenous IL-4 would induce the PV phenotype.

Although systemic corticosteroids and other immunosuppressants have been shown to reduce the mortality rate in PV patients, some cases are still refractory to these conventional therapies (29). Recent reports showing remarkable effects of biologics targeting molecules critically involved in the pathogenic process, such as TNF-α and IL-6, have resulted in dramatic changes in the treatment algorithms of several inflammatory diseases, including rheumatoid arthritis and Crohn's disease (30–32). Therefore, anti-IL-4 biologics are a potential therapeutic strategy for refractory PV. In this regard, humanized anti-IL-4 mAb and soluble IL-4Rα have already been manufactured for the treatment of allergic diseases, such as asthma, and shown to be well tolerated in clinical trials (33, 34). Further studies are necessary to evaluate the efficacy of anti-IL-4 biologics in patients with severe PV.

Acknowledgments

We are grateful to S. Koyasu (Keio University) for providing the Rag-2$^{-/-}$ OT-II transgenic mice, T. Randall and K. Kusser (Trudeau Institute) for advice on BrdU staining, S. Ito for mouse management, and M. Suzuki for the preparation of cryosections.

Disclosures

The authors have no financial conflicts of interest.